INVESTIGATION OF FENTON CATALYSTS SUITABLE FOR THE DEGRADATION OF AQUEOUS POLLUTANTS AT NEUTRAL pH

by

Alex Prevatte

Honors Thesis

Appalachian State University

Submitted to the Environmental Science Program

and The Honors College

in partial fulfillment of the requirements for the degree of

Bachelor of Science

May, 2017

Approved by:

_____

Michael Hambourger, Ph.D., Thesis Director

_____

Christopher S. Thaxton, Ph.D., Second Reader

_____

Christopher S. Thaxton, Ph.D., Departmental Honors Director

_____

Ted Zerucha, Ph.D., Interim Director, The Honors College

Table of Contents

List of Figures

List of Tables

List of Abbreviations

Allura Red	AR
Attenuated total reflectance	ATR
Chemical oxygen demand	COD
Distilled	DI
Disinfection by products	DBP
Environmental Protection Agency	EPA
Iron (II) tris(bipyridine-polydimethylsiloxane)	Febpy PDMS
Inductively Coupled Plasma Optical Emission Spectroscopy	ICP-OES
Insoluble inorganic matter	IIM
Insoluble organic matter	IOM
Instrument detection limit	IDL
Laboratory fortified blank	LFB
Organic wastewater contaminants	OWC
Parallel Climate Model	PCM
Reactive oxygen species	ROS
Round bottom flask	RBF
Soluble inorganic matter	SIM
Soluble organic matter	SOM
Suspended solid removal	SSR
Trihalomethanes	THM
Wastewater treatment plants	WWTP

Abstract

Unprecedented population growth has led to a resource constrained planet, with limited access to clean water. Many organic wastewater contaminants (OWCs) such as pharmaceuticals, hormones, and azo dyes are not removed by traditional methods of waste water purification, and are common in streams and rivers. The Fenton reaction, among other advanced oxidation processes, has been successfully used to degrade organic pollutants in waste water. This process traditionally requires a soluble iron catalyst and hydrogen peroxide oxidant at low pH. Neutral pH limits the solubility of iron, slowing the production of hydroxyl radicals. Based on a recent anomalous result within our own research group, the effect of pH on Fenton chemistry was revisited, confirming the established notion that the reaction proceeds most readily at low pH. To address this well-known limitation, an iron (II) tris(bipyridine-polydimethylsiloxane), FebpyPDMS, polymer coating was tested as a catalytic surface suitable for Fenton chemistry at neutral pH. Using this heterogeneous catalyst, it was observed that approximately 88% of the model pollutant, allura red (AR), was removed in one week. This work indicates that it is possible to degrade AR at neutral pH, though it is not as efficient as working under acidic conditions. IR difference spectra during the Fenton reaction suggested that the model pollutant was being degraded at multiple locations. Febpy PDMS may be reused repeatedly to remove pollutants from waste water during multiple treatments, possibly providing an affordable solution for tertiary water treatment.

I. Introduction

Clean Water Scarcity and Population Growth

Water is arguably the most important resource necessary for human life. In the developed world, human consumption patterns have played a pivotal role in water supply. As developing countries in the 18th and 19th centuries became industrialized, birth rates dramatically increased while death rates declined. In response to improved health care, technology, and living conditions, the global population has increased markedly post-industrialization. In response to unprecedented population growth in the 20th century, water resources have continued to be in high demand for residential, commercial, and industrial needs. In addition, per capita water consumption has increased which has further stressed water supplies. Currently, water deficiency is experienced by approximately four billion people at least one month out of the year [1]. By 2025, half of the world's population is projected to experience effects of water depletion [2]. As shown in Figure 1, water scarcity will be apparent in some regions more so than others.

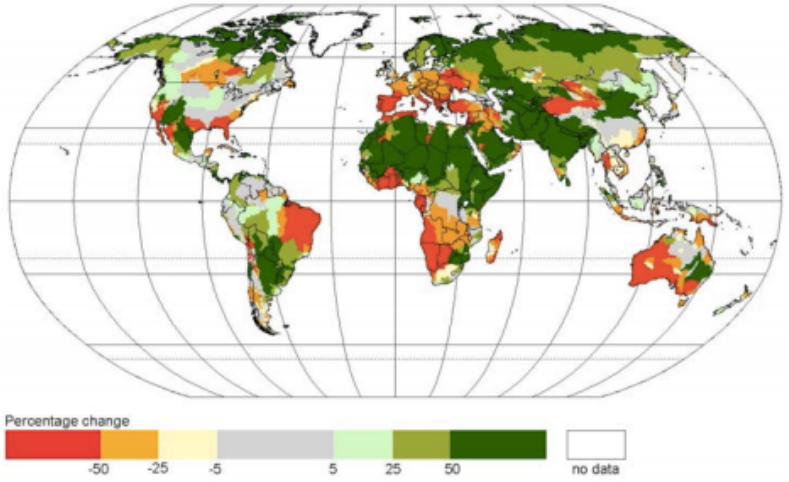

Figure 1. Global projection of water stress**.** Predicted change in water availability from 1961-1990 to the 2050s. Figure reproduced from [3].

Continued global population growth will likely lead to greater anthropogenic climate change, which can alter the dynamics of the hydrologic cycle in the future. The hydrologic cycle includes the reservoirs and fluxes of water through various processes including but not limited to evaporation, transpiration, and precipitation. Freshwater constitutes 2.5% of the total amount of water on Earth, and only a combined 31.3% of the freshwater content is stored in the subsurface and lithosphere [4]. The remaining supply of freshwater is contained within polar ice caps and glaciers, which is difficult to access. Warming of the Earth in recent decades has caused intense and extreme precipitation patterns, increasing evaporation, and changes in soil moisture and runoff [5]. These changes have put populations that depend on specific water resources, such as snow melt, at severe risk. During the last half of the twentieth century, the western United States experienced more winter precipitation falling as rain instead of snow [6]. The mean signal from the Department of Energy supported parallel climate model in 2008 indicated that human activities accounted for approximately 60% of the downscale trend in snow pack and decrease in river flow among seven states in the western U.S. It is evident that water reservoirs will be fluctuating with time, which has the potential to displace environmental refugees to population centers. In response to the shift in population distribution, increased stress will be placed on wastewater treatment.

To meet the demands for water consumption, many regions utilize groundwater resources. Groundwater has been exploited and continues to be widely used for drinking and crop irrigation [7]. Though most drinking water is sourced from surface water, groundwater is preferred because it is generally less contaminated. In areas that have limited precipitation and surface water supplies, groundwater pumping is much more prevalent. As water from aquifers is discharged, the recharge rate must balance the rate of discharge to prevent

substantial head declines. Mexico City, for example, has historically displaced the groundwater level by approximately 1-1.5 meters annually to supply its inhabitants [8]. If the water level declines without replacement, land subsidence will occur. The removal of pore water pressure from groundwater withdrawal causes increases in effective stress at the soil surface, which can lead to subsidence. Increases in groundwater pumping of the Chalco Basin in Mexico City due to water scarcity, has caused eight meters of land subsidence since 1991. As a result of excessive groundwater withdrawal, land subsidence has affected urban infrastructure, which has caused certain buildings to be more susceptible to failure in the presence of earthquakes and floods [9].

Another factor that dictates the condition and availability of freshwater is the state of contamination. Rivers, streams, and groundwater sources can be contaminated with heavy metals, pharmaceuticals, and other organic wastewater contaminants, OWCs [10]. Thousands of manmade chemicals produced in industrial and manufacturing processes have the ability to enter our water resources, and depending on the extent of regulation, some countries will have more polluted water sources than others. Point sources of water contamination include factory effluent from oil refineries and paper mills, which can be discharged directly into streams due to improper management. In the 1970s, the Environmental Protection Agency (EPA) regulated point source discharge to limit the amount of toxins in nearby water sources [11]. However, nonpoint source of water pollution has become more apparent. Hurricanes and flooding events can cause contaminates to travel by over wash, runoff, and groundwater infiltration. Contaminates can often travel long distances by advection and diffusion, which may enter freshwater sources that are sometimes unable to be purified.

Many OWCs are not removed by traditional methods of waste water purification, and are consequently discharged into surrounding streams and rivers. During rainfall events, storm water collects urban contaminants across impervious surfaces and can directly bypass waste water treatment by entering nearby surface and groundwater reservoirs. Though the concentrations of some OWCs in streams do not surpass expected drinking water guidelines in the U.S., some compounds, such as estriol and estradiol, are not naturally regulated in freshwater systems and have the potential to disrupt endocrine function [12]. Azo dyes also appear in waste water from dye manufacturing and textile waste. Though most dye compounds are not hazardous, some can produce toxic aromatic amine byproducts [13]. Therefore, improving the effectiveness of waste water treatment plants (WWTP) is in order to remove contaminants that can easily withstand traditional methods of water treatment. As a result, contaminated water sources can be remediated, and pristine water sources can remain intact.

Waste water treatment systems

Most wastewater treatment plants involve both primary and secondary treatment processes. Though the technologies and separation processes will differ slightly for each WWTP, the general purification scheme is relatively similar as depicted in Figure 2. Primary treatment is first used to mechanically separate insoluble inorganic matter (IIM) from soluble organic matter (SOM), insoluble organic matter (IOM), and soluble inorganic matter (SIM) [14]. As influent enters the treatment plant, IIM is physically removed through screens and grit chambers and taken to a separate location for further treatment. Via sedimentation soluble material is separated from insoluble material, to concentrate IOM. Soluble material and small IOM is contained within ‘overflow’ and is transported to secondary treatment.

Larger IOM makes up the ‘underflow’ during the sedimentation process, and is transferred to secondary biochemical treatment for stabilization and dewatering before being removed. During carbon oxidation, microorganisms consume SOM for energy and convert a fraction of the organic carbon into biomass while the remainder is fixed into carbon dioxide. The biomass is then separated using liquid/solid extraction, which successfully removes SOM. SIM such as ammonia is converted by nitrification and denitrification to produce nitrate and nitrogen gas respectively. After further physical treatment to remove secondary sludge, some WWTP incorporate various other treatment methods though they are not required in the U.S.

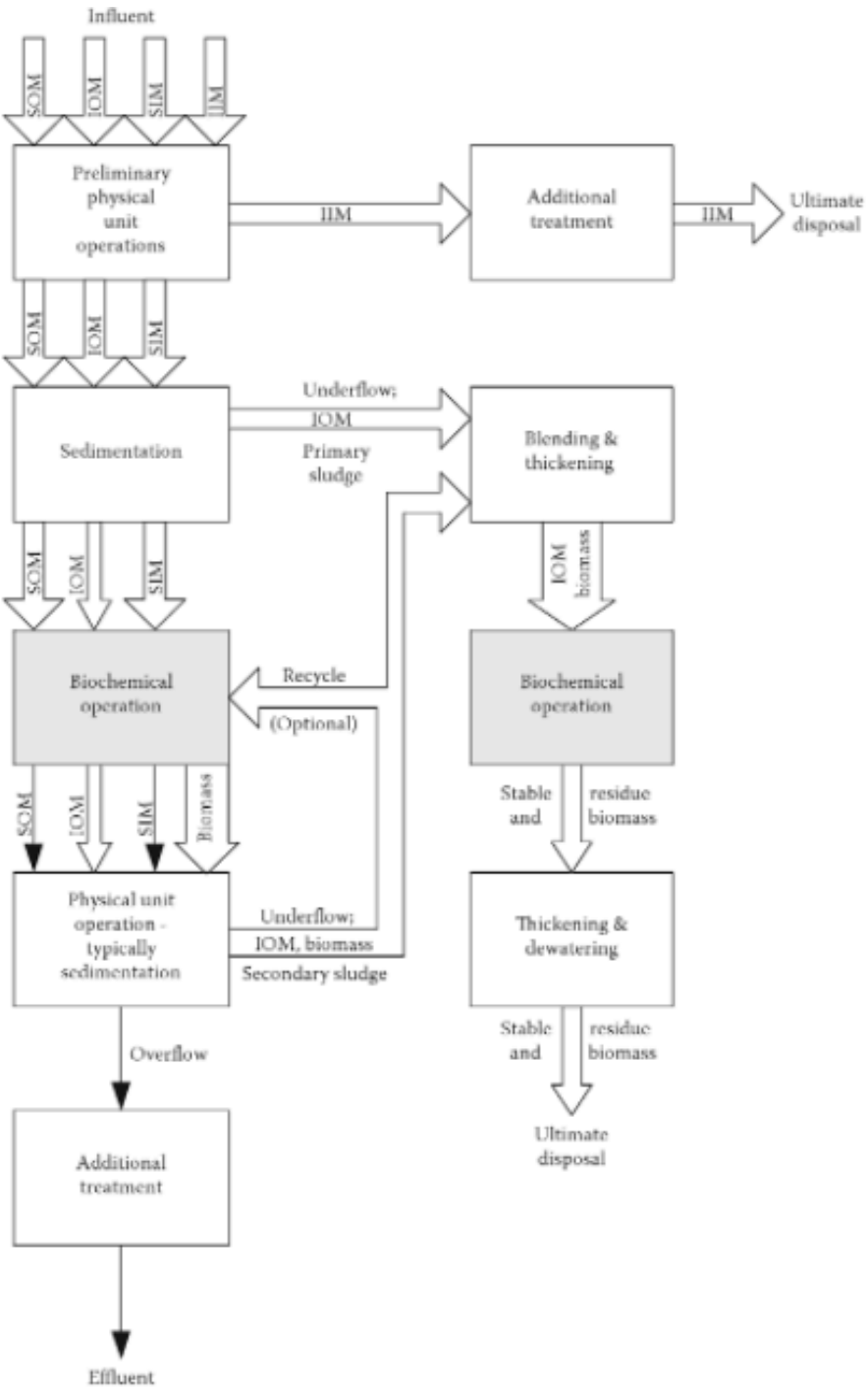

Figure 2. Traditional mechanism for waste water purification**.** Series of processes involving primary and secondary waste water treatment that is implemented in the majority of treatment plants. Figure reproduced from [14].

Tertiary treatment methods are used by WWTP, but can be of limited value. Some of the most common tertiary treatment methods include suspended solid removal (SSR), chlorination, and ozonation [14]. Many water disinfection methods such as these require large inputs of energy and capital, which limit their economic viability in WWTP. Chlorination is successful in removing most infectious microorganisms by introducing oxidants; however, it can produce toxic byproducts including organohalides such as trihalomethanes (THM). Ozonation utilizes ozone to further degrade pollutants, but can produce other disinfection by-products (DBPs) and is energy intesnive. The need for an efficient mechanism to degrade pollutants including their byproducts is apparent, especially in developing countries with less infrastructure and fewer resources. In recent years, water purification by the Fenton reaction has shown to be successful in degrading a wide array of contaminants that can easily pass through traditional methods of wastewater treatment.

Fenton chemistry

The Fenton reaction was discovered in 1876 by H.J.H. Fenton, with the addition of tartaric acid and hydrogen peroxide to a ferrous sulfate solution [15]. Fenton noticed the production of a violet color during the reaction, which was later found to be caused by the oxidation of tartaric acid, forming dihydroxymaleic acid. In the early twentieth century, Haber and Willstatter [16] proposed that hydroxyl radicals played a significant role in the iron-catalyzed decomposition of hydrogen peroxide. Hydroxyl radicals, among other reactive oxygen species (ROS), are powerful oxidants and have the ability to alter the chemical structure of organic compounds.

It was not until the late 1960s, that the Fenton reaction was applied in the degradation of organic pollutants such as azo dyes [13], recalcitrant pharmaceuticals [12],

and aromatic amines [17] in the wastewater treatment process. Other applications of the Fenton reaction include the elimination of water soluble pesticides [18], and the detoxification of total petroleum hydrocarbons in highly toxic soils. Ruppert & Bauer determined that UV light can be applied to promote the production of hydroxyl radicals through photoreduction of the ferric ion to ferrous ion [19]. Though the Fenton reaction can degrade many organic compounds, it has its limitations.

The Fenton reaction will work most efficiently under certain conditions. Ferrous iron, one of several catalysts that can be used in the reaction, must be in abundance to catalyze the degradation of the oxidant. Hence, ferrous iron must be soluble. The Pourbaix diagram shown in Figure 3, characterizes the different iron species that are present in water under varied conditions of pH and reduction potential [20]. Ferrous iron is most abundant under acidic conditions and a modest redox potential. Near neutral pH and upon the addition of an oxidant, precipitation of iron (III) will occur. An example of an iron (III) species that may form is Fe_2O_3 as depicted below in Figure 3. This is one of the shortcomings of the homogeneous Fenton reaction, as the catalytic ferrous iron will be unavailable to drive the reaction near neutral pH. In order for ferric iron to catalyze the Fenton reaction, the concentration of iron must be between 50-80 ppm which is above the standard for the amount that can be discharged into the environment [21]. In most instances, the solution must be acidified to achieve these high concentrations. This is significant because as waste water effluent leaves the system, the pH must be brought back up to neutral. The acidic pH requirements for Fenton chemistry, versus the acceptable near neutral pH range for water discharge, adds additional costs and complexity that limits the application of the Fenton reaction as a method for tertiary waste water treatment.

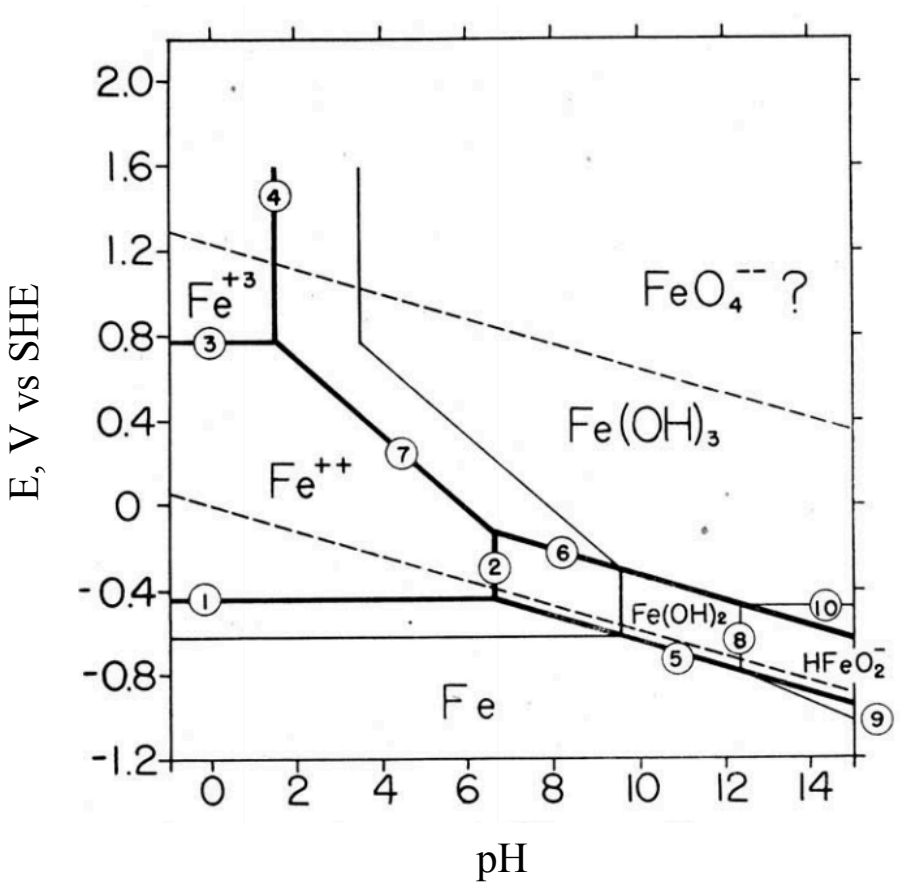

Figure 3. Pourbaix diagram of iron. Distribution of iron species with redox potential vs. pH. Each number represents a chemical reaction interconnecting between the two species separated by that line. This is a significant limitation to using iron as a catalyst in the Fenton reaction. Image reproduced from [20].

Heterogeneous Fenton reaction

Immobilizing the ferrous iron catalyst onto packed beds, membranes, or other surfaces can be used to successfully degrade pollutants from water. This method can be beneficial as it prevents the catalyst from leaching into the solution while catalyzing the decomposition of the oxidant, and therefore the target pollutant. The heterogeneous catalyst can be reused in most scenarios since desorption of products at the active site occurs after the reaction has taken place. This leaves active sites available for continual adsorption of reactant compounds during the reaction, making it very cost effective in the waste water treatment

process. One of the drawbacks to this method however, is that surface catalysts may have less efficient interactions with the oxidant due to limited interfacial surface area. Since only the outer layer of the catalyst comes into contact with the waste water, the amount of ferrous iron available for reaction may be limited. Figure 4 Depicts the synthesis of iron (II) tris(bipyridine-polydimethylsiloxane), Febpy PDMS, with crosslinking of bipyridine-terminated PDMS chains to make the material. In this work, Febpy PDMS was tested as an immobilized catalyst for the Fenton reaction. The material can adhere to glassware, while the ferrous iron center interacts with hydrogen peroxide to produce hydroxyl radicals.

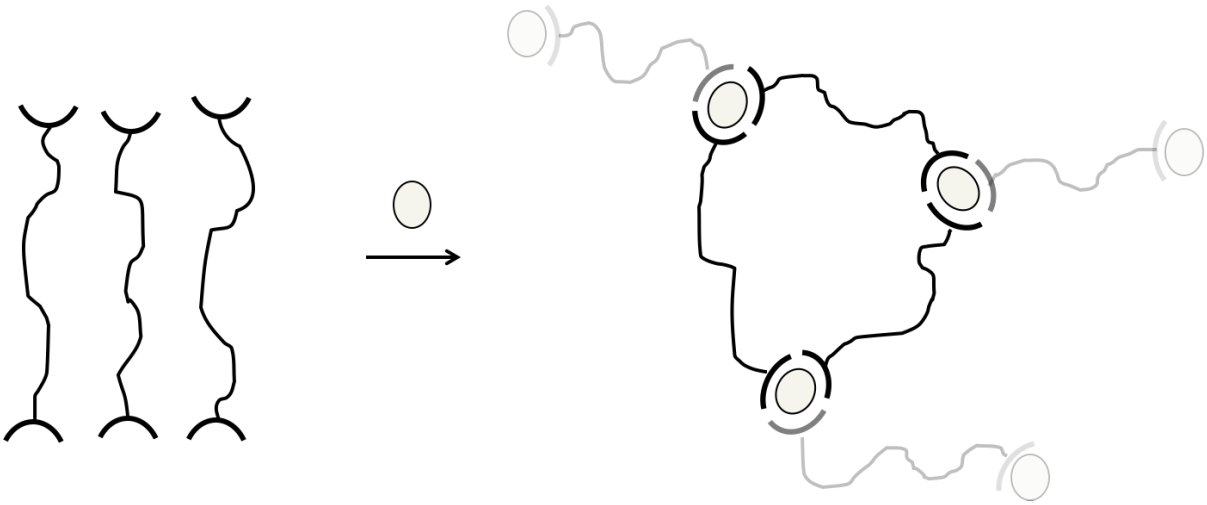

Figure 4. Febpy PDMS polymer formation. Reacting bpyPDMS with iron (II) tetrafluoroborate, $Fe(BF_4)_2$ under anaerobic conditions, yields Febpy PDMS. Thanks to Dr. Al Schwab for the reaction scheme depiction.

Fenton reaction mechanism

The Fenton reaction mechanism is not completely understood in the literature. The traditional understanding involves iron catalyzed decomposition of hydrogen peroxide, yielding hydroxyl radicals and other radical species. This radical mechanism includes the addition of catalytic ferrous iron ions (Fe^{2+}) to an acidic solution in the presence of hydrogen

peroxide (H_2O_2) to produce ferric iron ions (Fe^{3+}), hydroxyl radicals ($OH\bullet$) and hydroxide (OH^-) as shown in equation one [21].

$$Fe^{2+} + H_2O_2 \rightarrow Fe^{3+} + OH\bullet + OH^- \quad (1)$$

The production of hydroxyl radicals in this initiation step results in a sequence of cascading reactions (Equations 2-5). Hydroxyl radicals can react with hydrogen peroxide to produce water and peroxyl radicals ($HO_2\bullet$) (Equation 2). Peroxyl radicals can then react with ferrous iron to generate ferric iron and hydroperoxide anion (HO_2^-) (Equation 4), or can react with ferric iron to produce ferrous iron and hydroxide (Equation 3).

$$OH\bullet + H_2O_2 \rightarrow H_2O + HO_2\bullet \quad (2)$$

$$Fe^{3+} + HO_2\bullet \rightarrow Fe^{2+} + O_2 + H^+ \quad (3)$$

$$Fe^{2+} + HO_2\bullet \rightarrow Fe^{3+} + HO_2^- \quad (4)$$

$$Fe^{2+} + OH\bullet \rightarrow Fe^{3+} + OH^- \quad (5)$$

Hydroxyl radicals will further react with organic substrates (RH), abstracting a proton, and producing organic radicals ($R\bullet$) as shown in equation six. These organic radicals are extremely reactive, and can be further oxidized as observed in equations 7 and 8 below [22].

$$RH + OH\bullet \rightarrow H_2O + R\bullet \quad (6)$$

$$R\bullet + H_2O_2 \rightarrow ROH + OH\bullet \quad (7)$$

$$R\bullet + O_2 \rightarrow ROO\bullet \quad (8)$$

These organic radicals can further react to continue radical chemistry, until a termination step in which the organic free radicals can then either be oxidized by Fe^{3+}, reduced by Fe^{2+}, or dimerised, as shown in equations 9, 10, or 11, respectively.

$$R\bullet + Fe^{3+} \rightarrow R^+ + Fe^{2+} \quad (9)$$

$$RH + Fe^{2+} \rightarrow R^- + Fe^{3+} \quad (10)$$

$$2R\bullet \rightarrow R\text{-}R \quad (11)$$

The reaction is not limited to the involvement of iron as the catalyst, as many other first row transition metals can also serve as catalysts. The mechanism is carried out similarly with the involvement of the reduced (M^{n+}) and oxidized state (M^{n+1}) of the catalyst (Equation 12).

$$(M^{n+}) + H_2O_2 \rightarrow (M^{n+1}) + OH\bullet + OH^- \quad (12)$$

Contrary to this widely accepted series of reactions, an alternative mechanism has been postulated, invoking a ferryl iron species [21]. This alternative mechanism proceeds with the reversible formation of a primary intermediate with the exchange of H_2O, followed by the formation of the ferryl ion by the loss of H_2O (Equation 13). This species can either react with ferrous iron to produce ferric iron, or with hydrogen peroxide to produce oxygen (Equations 14 and 15). The highly oxidizing ferryl species could also directly oxidize organic components in the solution.

$$Fe^{2+} + H_2O_2 \rightarrow [\, Fe^{2+} \cdot H_2O_2] \rightarrow FeO^{2+} \quad (13)$$

$$FeO^{2+} + H_2O_2 \rightarrow Fe^{2+} + O_2 + H_2O \quad (14)$$

$$FeO^{2+} + Fe^{2+} \rightarrow 2Fe^{3+} + 2OH^- \quad (15)$$

It is experimentally difficult to determine which reaction pathway is most favored in the Fenton reaction. Recent computational studies on the free energy pathways of both reactions were performed, suggesting that the ferryl-oxo species is more energetically favored in comparison to the reaction producing a hydroxyl radical [23]. Although the production of the ferryl-oxo species requires two steps, it does not need to undergo the energy barrier in the one step process involved in hydroxyl radical production. This may indicate that the ferryl species is the primary oxidizing agent over the hydroxyl radical.

Project Outlook

The Fenton reaction involving soluble and immobilized iron catalyst was investigated to determine the efficacy of organic pollutant degradation. The Fenton reaction has been widely used for waste water purification, and this project focuses on determining a promising method to degrade AR at neutral pH. Recent research in lab suggested that AR dye degradation was optimal at neutral pH [24]. There was also an indication that solutions containing pH 7 phosphate buffer had removed the most AR dye absorbance in comparison to pH 3 and 5 buffered solutions. According to the literature, the Fenton reaction works best at low pH ranges to maintain the quantity of catalytic ferrous iron in solution. Ferrous iron in the presence of more neutral conditions, leads to precipitation of ferric iron species which will not catalyze the decomposition of hydrogen peroxide to produce hydroxyl radicals.

This project aims to determine the optimal conditions for Fenton chemistry by investigating pH effects with and without phosphate buffer to follow recent results in the research lab. AR degradation was monitored using UV-vis spectroscopy to follow the decrease in absorbance at the peak wavelength as an indicator of pollutant removal. Iron concentration series were then examined to compare the rate of the reaction in pH 3, 5, and 7, solutions both in the presence and absence of phosphate buffer. To address the issue of successfully performing the Fenton reaction at neutral pH, Febpy PDMS was tested as a heterogeneous Fenton catalyst The performance of this catalyst in the removal of the pollutant was examined by comparing absorbance degradation for replicate coatings. To further analyze the extent of removing the model pollutant, IR spectroscopy was used to monitor the difference spectra of chemical constituents in AR over time.

II. Experimental

Reagents

Ferrous sulfate heptahydrate was purchased from J.T. Baker Chemical, Columbus, Ohio. Distilled (DI) water was used from faucets in the research facility. Hydrogen peroxide (36%), sodium dihydrogen phosphate buffer solutions, iron (II) tetrafluoroborate, $Fe(BF_4)_2$, and allura red were manufactured by Sigma Aldrich, St. Louis, Missouri. Ferric chloride hexahydrate and sodium hydroxide was purchased from Mallinckrodt, St. Louis, Missouri. HCl and THF were manufactured at EMD, and toluene was manufactured at BDH.

Instrumentation

UV-visible spectra were obtained with a 3 mL 1-cm path length quartz cuvet using either a Shimadzu UV-2401 or Shimadzu UV-2600 spectrophotometer. Allura red solid, Fenton reaction aliquots, and iron phosphate material were measured on a Nicolet 6700 FTIR spectrometer with an attenuated total reflectance element (Smart iTR). The Varian 710-ES ICP Optical Emission Spectrometer (069342) was used on Febpy PDMS filtrate solutions to determine the quantity of iron that had leached into solution. To adjust the pH of each solution, an Orion 710 A pH meter was used with an accunet gel filled probe (# 13-620-108A). A Mettler Toledo AT200 analytical balance was used to quantitatively measure reagents used in the experiments.

Febpy PDMS Synthesis

Approximately 45.4 mg of 100cSt bipyridine PDMS was weighed into a 25-mL round bottom flask (RBF) and mixed with 1 mL of anaerobic THF under nitrogen atmosphere. In a separate solution, 1.63 mg/mL of $Fe(BF_4)_2$, was mixed in 1 mL of anaerobic THF. The 1 mL of iron stock was then transferred anaerobically to the 1 mL of bipyridine

PDMS solution with a syringe. The solution turned red instantly. Then, the solvent was evaporated under nitrogen gas while gently heated. Approximately 1.4 mL of toluene was used to redissolve the Febpy PDMS to yield 4 weight percent of material. The solution was filtered through a 0.45 micro PTFE syringe filter, and different volumes were added to RBFs followed by gentle heating until toluene evaporated. Each RBF was then placed in the drying oven overnight at 100 °C to coat the Febpy PDMS onto the flasks.

Procedures

Soluble and Immobilized Fenton Reaction

Samples of 100 mL were prepared with 0.98 mM iron catalyst and 0.02 mM AR in DI water. The reaction was initiated with the addition of 86 uL of 36% hydrogen peroxide to yield a final concentration of 9.98 mM while being stirred. Differences in pH were tested with pH adjusted DI water or 0.1 M phosphate buffer at approximately pH 3, 5, and 7. Phosphate buffer and DI water were pH adjusted using 6 M HCl, 3 M NaOH, and the pH meter. The reaction rate was then examined under a range of catalyst concentrations including 0.50 mM, 0.18 mM, 0.018 mM, 0.0090 mM, and 0.0018 mM ferrous sulfate, while maintaining the same oxidant concentration. Solutions coated with immobilized Febpy PDMS contained 0.02 mM of AR, and were initiated with 9.98 mM addition of 36% concentration of hydrogen peroxide in a 25 mL RBF. The sample was adjusted to near neutral pH using 6 M HCl, 3 M NaOH, and the pH meter.

To determine the extent of AR degradation, UV-visible spectrophotometry was used to monitor changes in absorbance at 502 nm. About 3 mL of solution was pipetted into a quartz cuvette for measurement, and was transferred to waste thereafter. For Febpy PDMS tests, each aliquot was returned to the stirred reaction flask after UV-vis measurement. This

was due to the smaller volume of sample. Aliquots from solutions containing both the homogeneous and immobilized catalysts were taken for short and long time intervals to determine the reaction rate. The absorbance readings were all baselined on DI water.

ICP-OES Analysis

After performing the Fenton reaction using immobilized Febpy PDMS, ICP was used to determine if iron had leached into solution. The Febpy PDMS samples were filtered and acid digested in approximately 10 mL of HNO_3 before being analyzed. Then, an iron calibration curve was produced using 0 ppm, 0.05 ppm, 0.5 ppm, 1ppm, 5ppm, and 50 ppm iron standards. The triplicate absorbances of all Febpy PDMS filtrates were averaged. The average absorbances were then converted to concentration to determine the concentration of iron in solution. A 20 ppm laboratory fortified blank (LFB), and a 5ppm instrument detection limit (IDL) were measured to determine measurement reliability and instrument sensitivity respectively.

IR Analysis

IR spectroscopy was used to characterize the iron phosphate material that was produced in the Fenton reaction involving phosphate buffer. The reaction took place in a 3 mL cell with 0.02 mM AR, 0.98 mM ferrous sulfate, and 9.98 mM of hydrogen peroxide in pH 7 phosphate buffer. An aliquot of the solution was placed under the diamond ATR element, and was locked in place to measure the IR spectrum.

To monitor changes in the chemical structure of AR, an IR spectrum of solid AR was compared with that of aqueous AR at different time intervals during the reaction. The solution was prepared with 0.2 mM AR, 0.50 mM ferrous sulfate, and was initiated with 9.98 mM of hydrogen peroxide in 100 mL of DI water. The difference spectrum was determined

for the AR structure over time, and peaks were further analyzed to determine changes in bond vibrations.

III. Results

Preliminary Fenton Testing

The absorption spectrum of AR dye at 502 nm before and after the Fenton reaction is depicted below in Figure 5. The peak absorbance was monitored as the Fenton reaction progressed to determine the extent of dye decolorization.

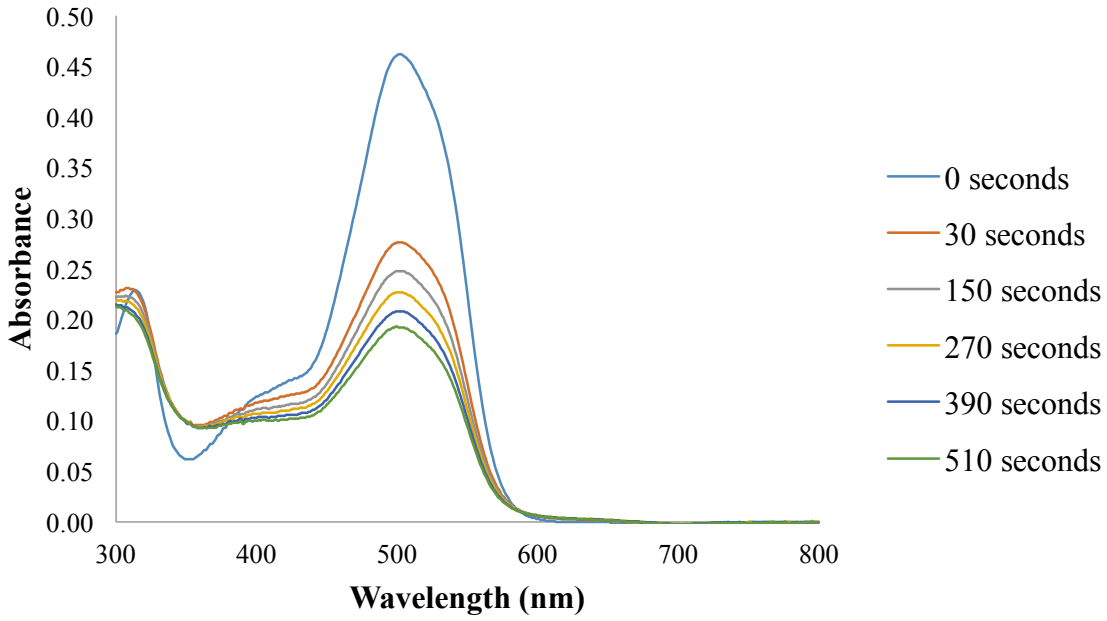

Figure 5. Absorption spectrum of AR during the Fenton reaction. The change in absorbance was monitored after the addition of hydrogen peroxide to a concentration of 9.98 mM in 100 mL of pH 3 solution containing 0.02 mM AR and 0.18 mM of ferrous sulfate. The pH of the solution was adjusted after the addition of ferrous iron and AR.

Fenton reaction controls were then performed to test for variations in absorbance. After measuring the absorption spectrum for all of the controls, it was noticed that scattering was involved in solutions that had a higher pH, or in the presence of phosphate with ferrous sulfate as shown in Figure 6.

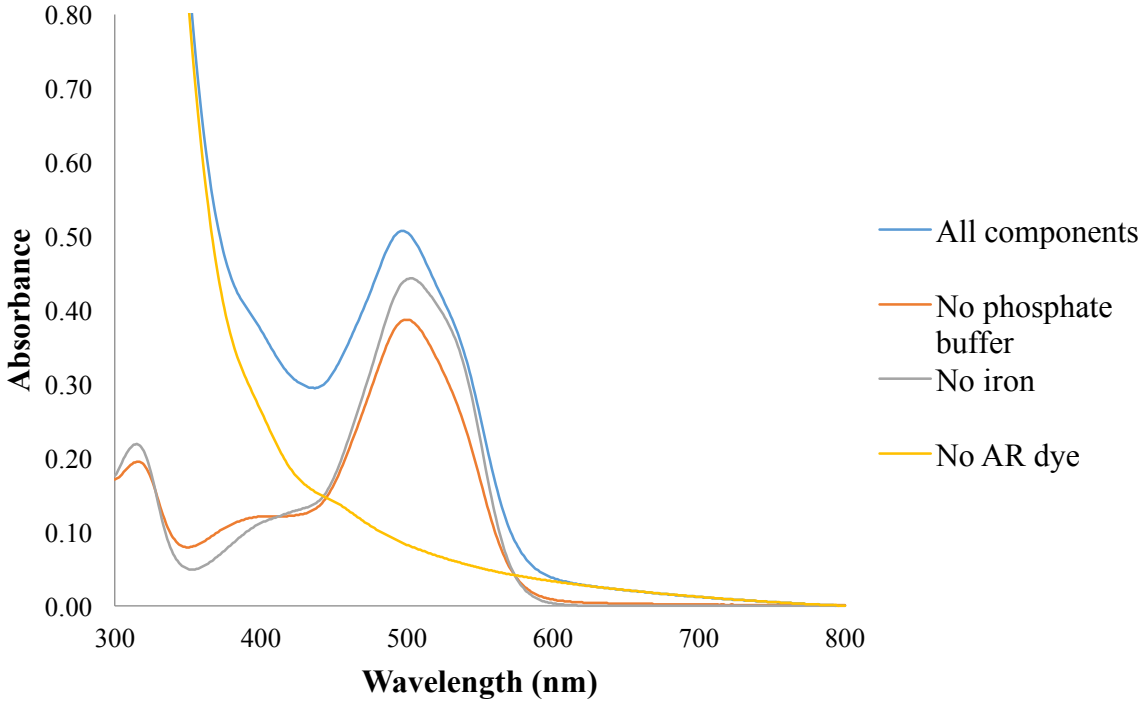

Figure 6. Fenton reaction controls in pH 5 solution. The all components series contained 80 mM of pH 5 phosphate buffer, 0.02 mM AR, and 0.98 mM ferrous sulfate. Controls were performed with the indicated component missing. All runs were performed in 100 mL of solution.

In solutions containing high concentrations of ferrous sulfate (0.98 mM), scattering was present in the absorption spectrum as the reaction was initiated. The presence of scattering is indicated by the exponential curves at all times points excluding zero seconds in Figure 7.

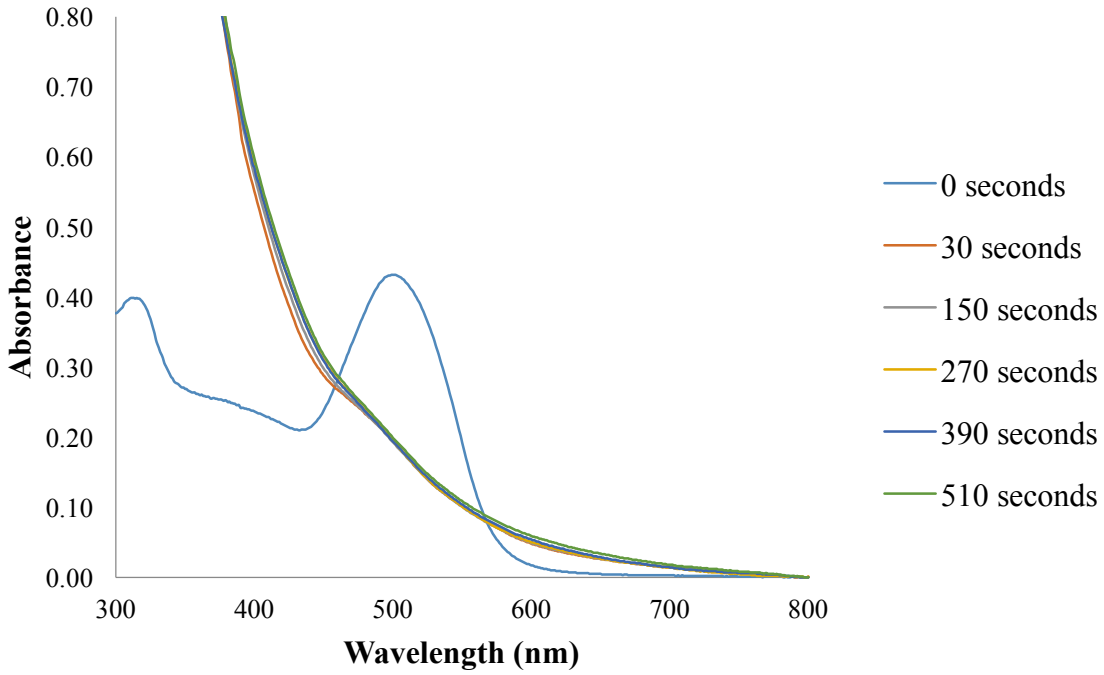

Figure 7. Absorption spectrum of AR in the presence of 0.98 mM ferrous sulfate**.** The change in absorbance was monitored after the addition of hydrogen peroxide to a concentration of 9.98 mM in 100 mL of pH 5 solution containing 0.02 mM AR. The zero second time series indicates the absorption spectrum of the solution before the addition of hydrogen peroxide, while the remaining time series are measured after the reaction was initiated.

To account for the presence of scattering in absorption spectra for samples containing 0.98 mM ferrous sulfate, an exponential curve was fit to the data as observed in Figure 8, and the absorbance due to light scattering at 502 nm was subtracted from the peak absorbance.

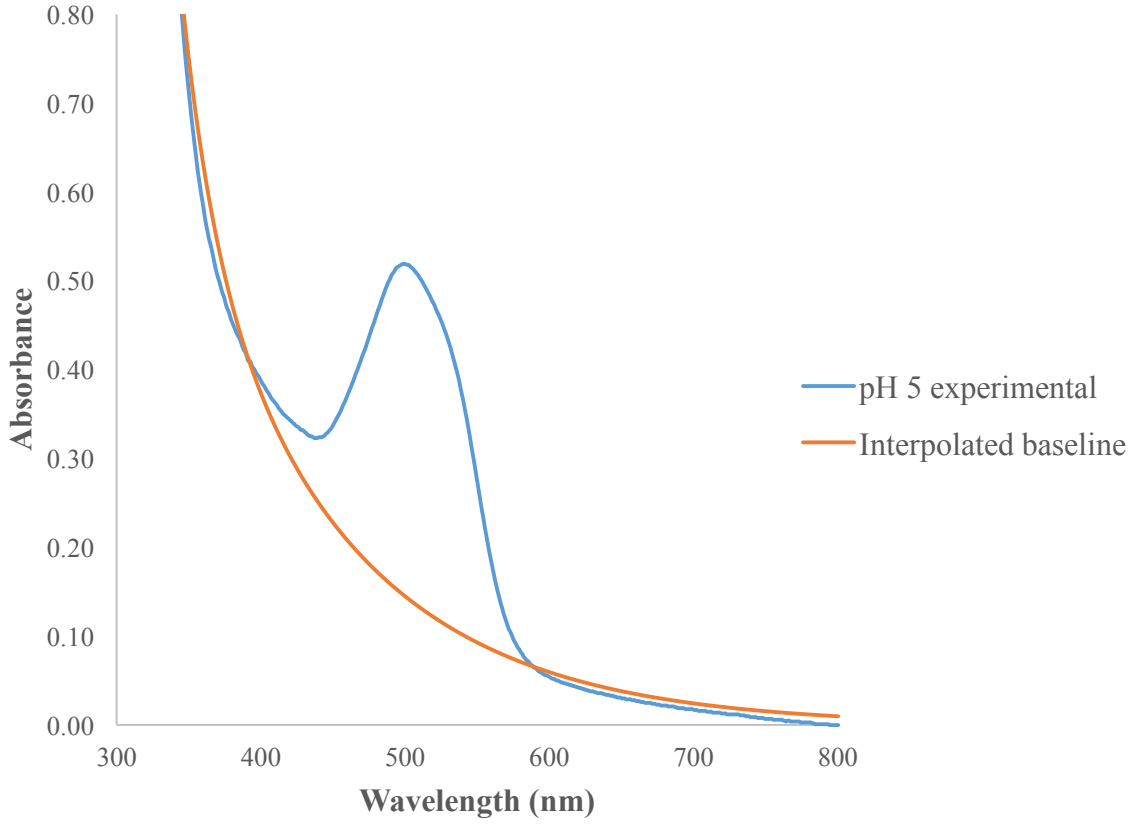

Figure 8. Absorption spectrum of AR in pH 5 buffer with exponential curve fit. Scattering due to precipitation of iron (III) material was evident upon initiation of the Fenton reaction. An exponential line was fit to correct A_{502} for scatter.

Iron phosphate particles precipitating out of phosphate buffered solution were characterized using IR spectroscopy. The literature IR spectrum of iron (III) phosphate in Figure 9, was compared to that of the IR spectrum of the material collected by filtration of the solution, which is depicted in Figure 10.

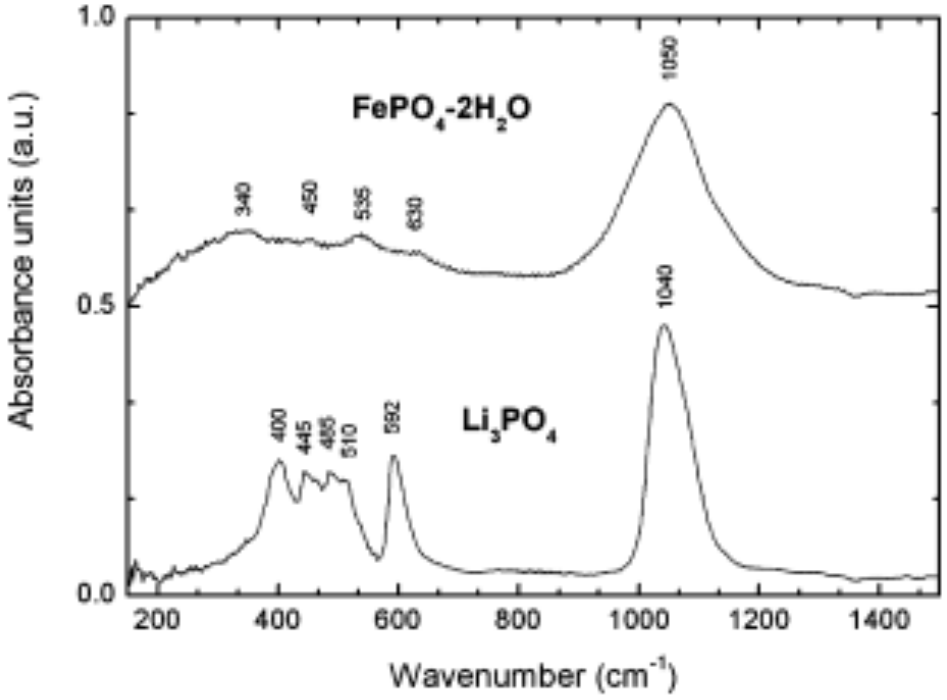

Figure 9. Literature IR spectrum of $FePO_4 \bullet 2H_2O$**.** The spectrum on the top displays one definitive peak at 1050 cm^{-1} for the compound. Figure reproduced from [25].

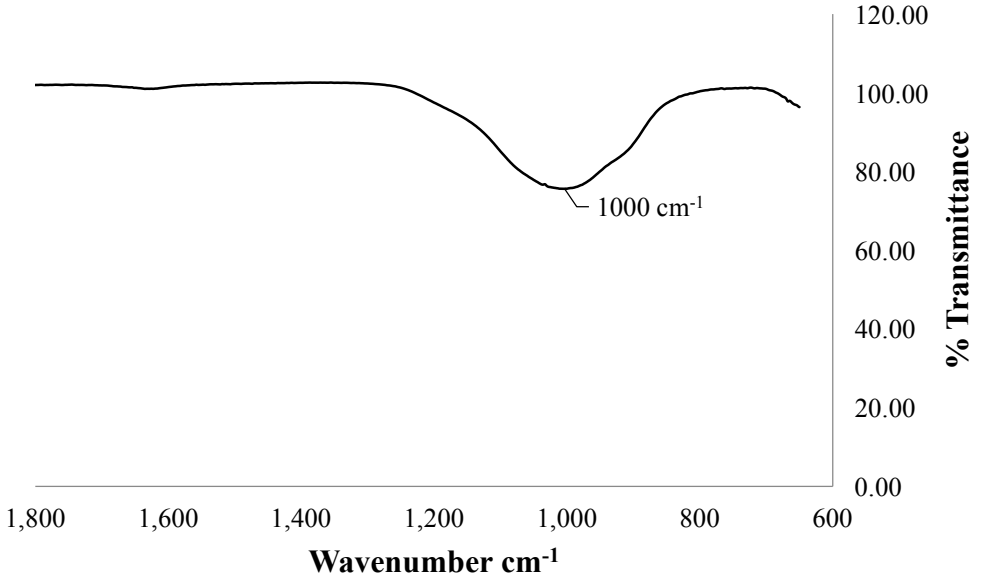

Figure 10. IR spectrum of iron phosphate precipitate isolated from buffered reaction. It is likely that the material formed was iron (III) phosphate due to the formation of the broad peak at 1000 cm^{-1}.

The degradation of AR at 502 nm was then investigated at various pH levels to determine the ideal conditions for dye removal as shown in Figure 11. In the pH 3 solution containing 0.98 mM ferrous sulfate, most of the AR was removed within 30 seconds. By 390 seconds, 100% of the AR dye was degraded. At the same time interval, pH 5 and pH 7 solutions experienced 80% and 6% dye removal respectively. The pH 5 and 7 solutions contained cloudy precipitate after the addition of hydrogen peroxide.

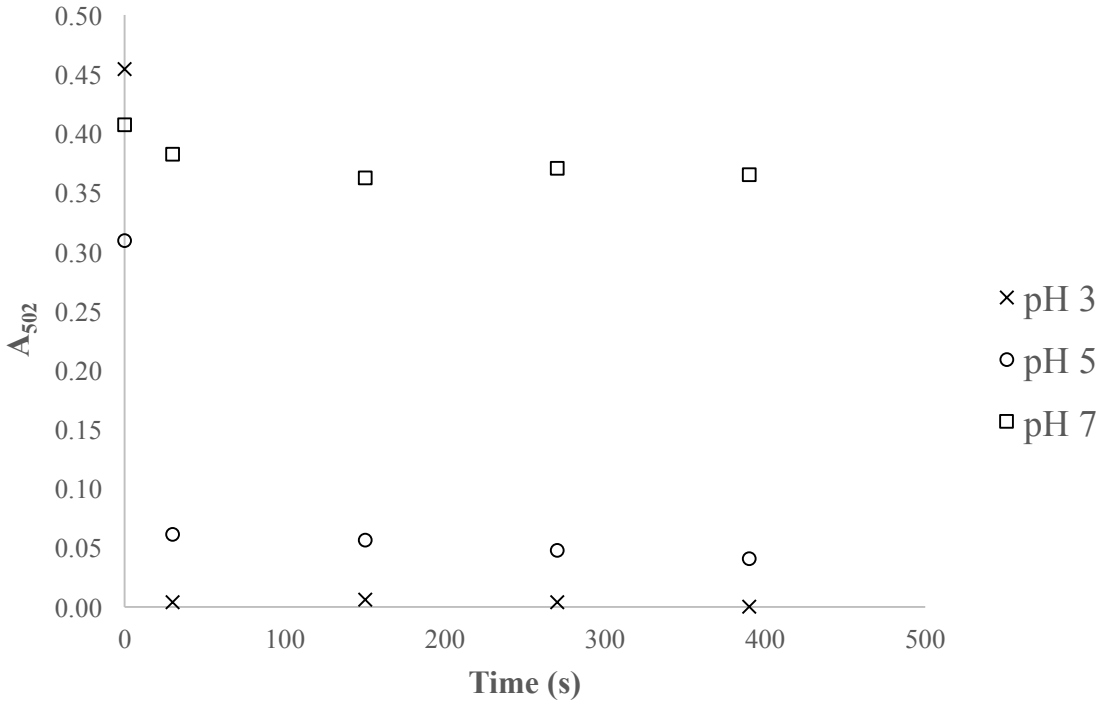

Figure 11. Kinetic traces of AR decolorization at various pH in the absence of phosphate buffer**.** The change in absorbance was monitored after the addition of hydrogen peroxide to a concentration of 9.98 mM in 100 mL of solution containing 0.02 mM AR and 0.98 mM of ferrous sulfate. The pH of each solution was adjusted after the addition of ferrous iron and AR. Initial time points were measured for each solution, as well as 30-second, 150-second, 270-second, and 390-second time points.

The influence of 80 mM phosphate buffer was tested on 0.98 mM iron solutions at pH 3, 5, and 7 in Figure 12. It was determined that dye decolorization is most efficient in pH 3 phosphate buffer. In 390 seconds, there was no dye degradation in the pH 7 buffered solution. At the end of the time interval, the pH 3 solution had experienced 96% dye removal, while the pH 5 and pH 7 solutions experienced 60% and 20% dye removal respectively.

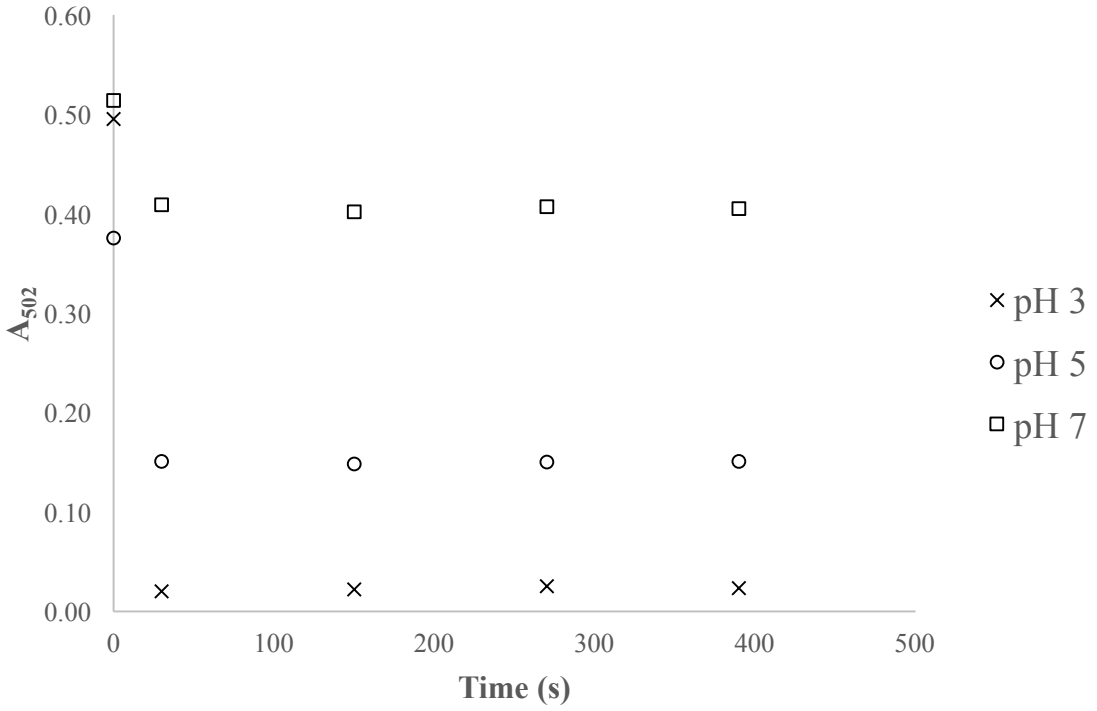

Figure 12. Kinetic traces of pH series in 80 mM phosphate buffer**.** The change in absorbance was monitored after the addition of hydrogen peroxide to a concentration of 9.98 mM in 100 mL of solution containing 0.02 mM AR and 0.98 mM of ferrous sulfate. Each solution was adjusted to either pH 3, 5, or 7 in 80 mM sodium phosphate buffer. Initial time points were measured for each solution, as well as 30-second, 150-second, 270-second, and 390-second time points.

Determining the rate of the Fenton reaction

The kinetics of the Fenton reaction were monitored at various iron concentrations to determine minimum iron loading required under various conditions. In pH 3 solution, the 0.50 mM and 0.18 mM iron solutions degraded AR most quickly as depicted in Figure 13. Both solutions had completely removed AR in one hour, and the remaining samples degraded AR within 48 hours. The iron control solution which lacked iron catalyst, experienced slight degradation in one day, however the absorbance was not decreased significantly. Unfortunately, the absorbance of the control was not monitored after 48 hours.

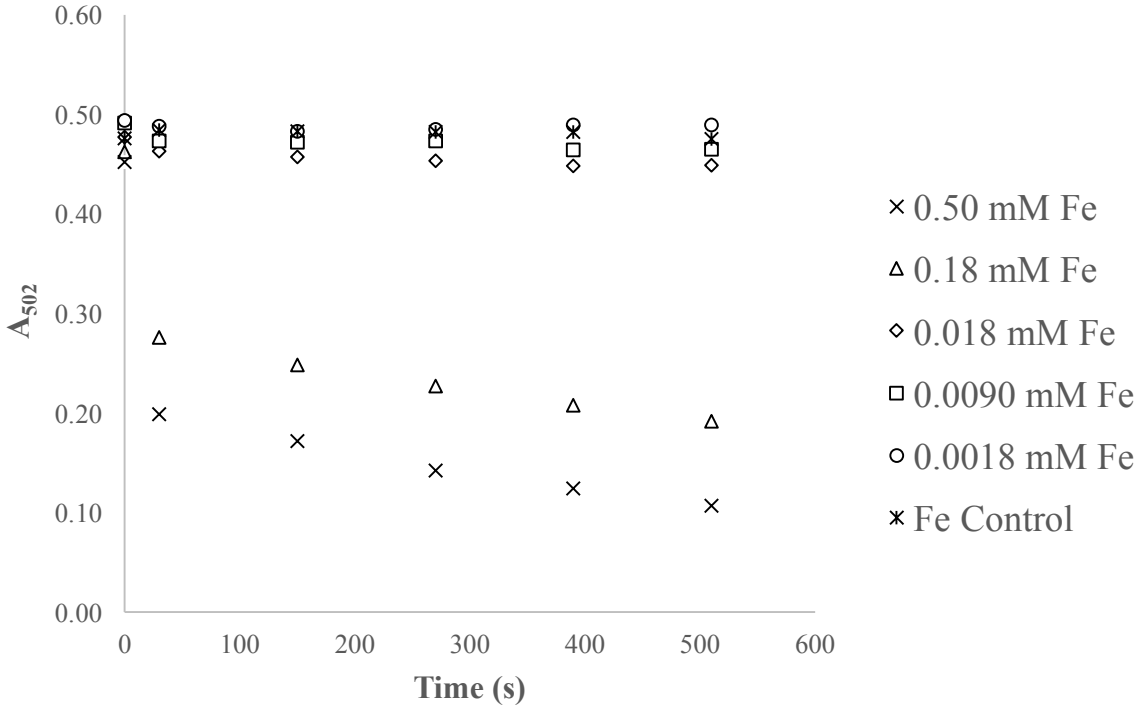

Figure 13. AR decolorization for pH 3 iron series in DI water within 510 seconds. AR decolorization with various concentrations of iron. The 100 mL solutions contained equal concentration of AR (0.02 mM) and H_2O_2 (9.98 mM).

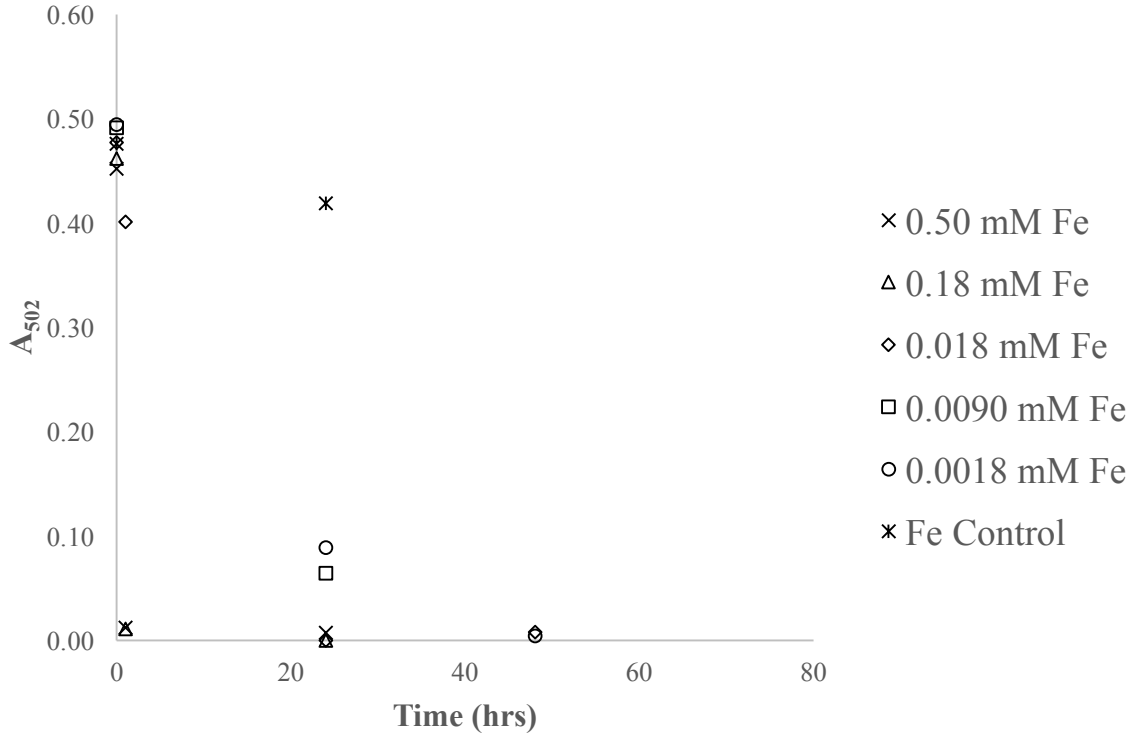

Figure 14. AR decolorization for pH 3 iron series in DI water within 48 hours. This graph is a continuation from Figure 13 for 48 hours.

Phosphate pH 3 buffer was incorporated at both short and long time durations to compare differences in AR absorbance with pH 3 adjusted DI water in Figures 15 and 16 respectively. The 80 mM pH 3 buffered iron series showed proportional decreases in absorbance upon the addition of hydrogen peroxide at 30 seconds. The reaction slowed dramatically thereafter for all solutions, limiting the capability for complete AR decolorization.

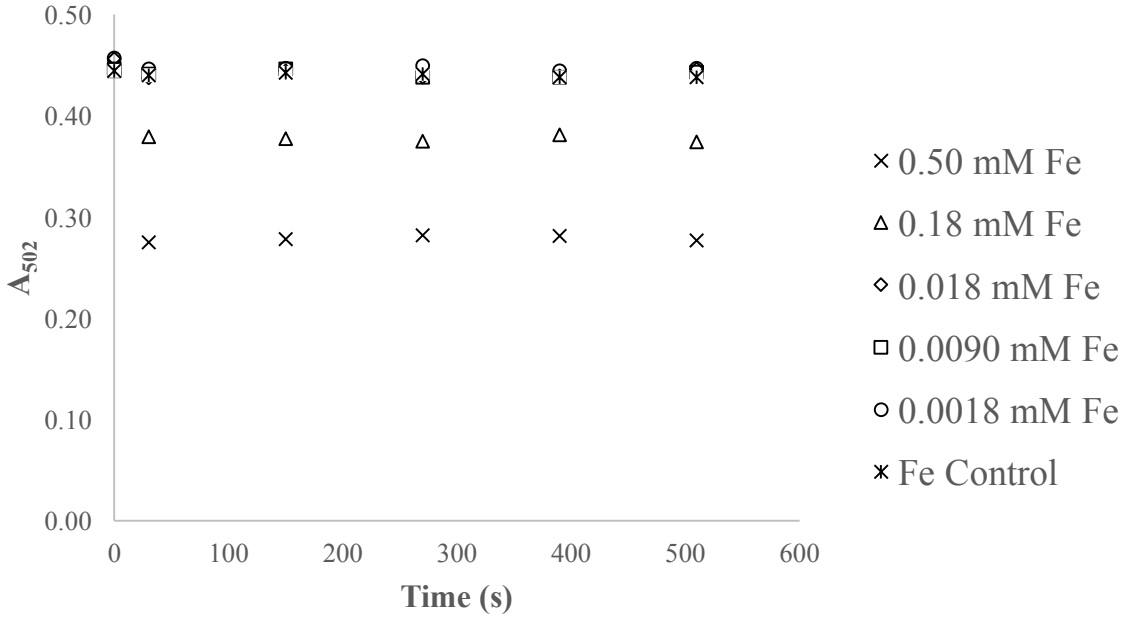

Figure 15. AR decolorization for buffered pH 3 iron series in short duration**.** AR decolorization in 24 hours with various concentrations of iron in pH 3 phosphate buffer. The 100 mL solutions contained equal concentration of AR (0.02 mM) and H_2O_2 (9.98 mM).

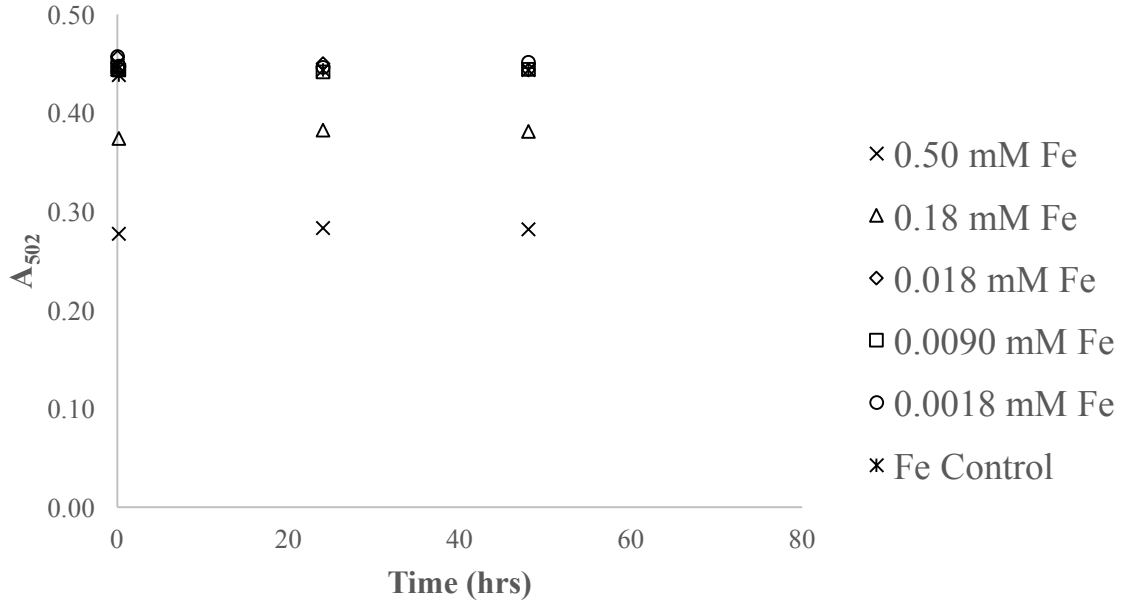

Figure 16. AR decolorization for buffered pH 3 iron series in 48 hours. This graph expands from Figure 15 by showing the continued degradation of AR in 48 hours at 502 nm.

An iron series for the Fenton reaction in pH 5 DI water and buffer was also investigated to determine differences in the rate of the reaction in Figures 17-20. In pH 5 DI water, the 0.50 mM solution nearly degraded entirely after 48 hours with approximately 94% dye removal. The 0.18 mM, 0.018 mM, 0.0090 mM, and 0.0018 mM iron solutions had removed about 79%, 54%, 53%, and 48% of AR dye respectively. The iron control for the pH 5 DI water solution experienced only slight degradation in two days.

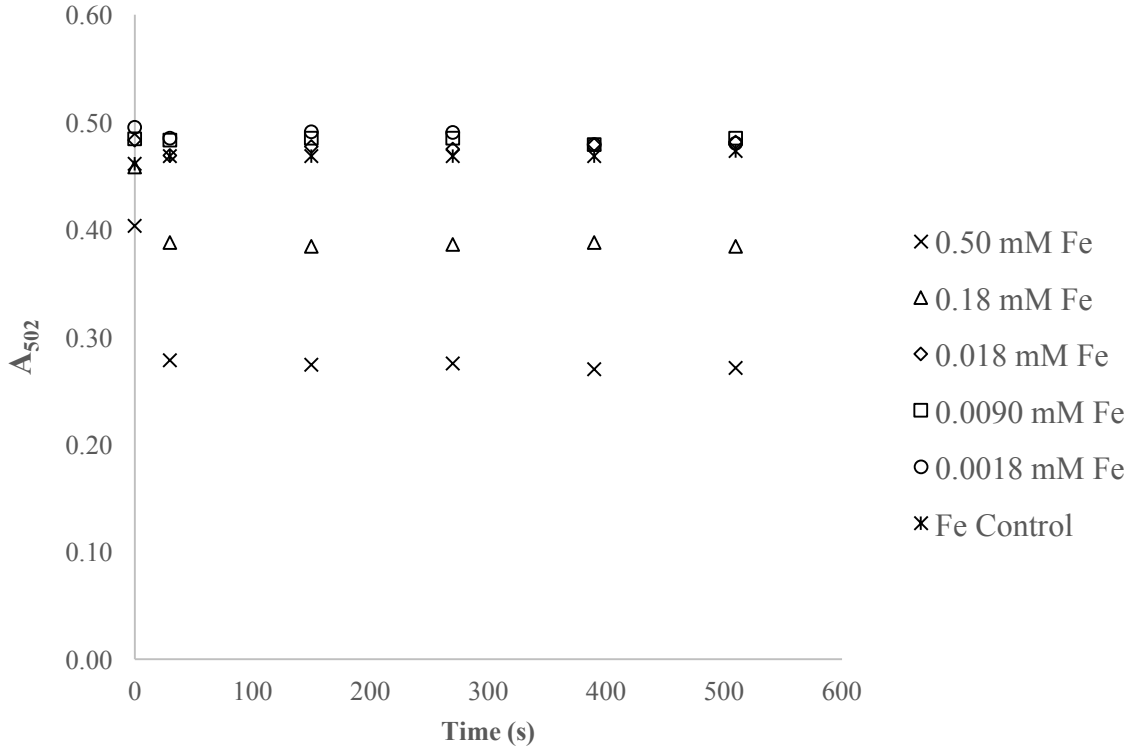

Figure 17. AR decolorization for pH 5 iron series in short duration**.** The degradation of AR, monitored by peak absorbance at 502 nm, as a function of time for different iron concentrations. The AR absorbance quickly decreased when the reaction was initiated, and then remained essentially constant over time.

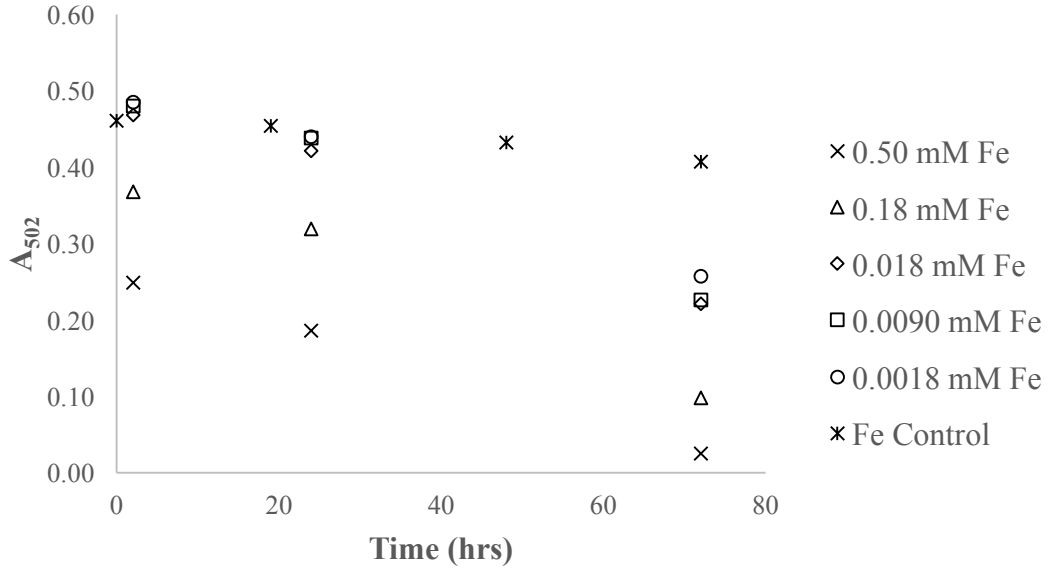

Figure 18. AR decolorization for pH 5 iron series in 72 hours. This graph is a continuation from Figure 17. Dye absorbance decreased significantly for the solutions containing 0.50 mM and 0.18 mM iron. The degradation of AR for lower concentrations of iron was less substantial.

In 80 mM pH 5 phosphate buffer, the 0.50 mM degraded the most within 30 seconds. Thereafter, the AR in each iron solution was stable over the next 24 hours.

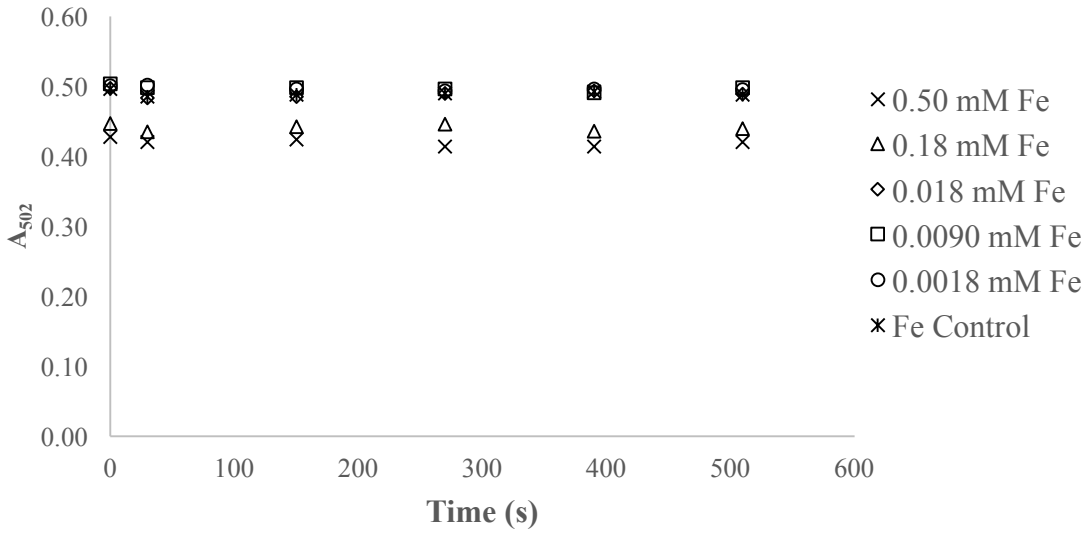

Figure 19. AR decolorization for buffered pH 5 iron series**.** Slight decolorization of AR for the duration of 8.5 minutes at 502 nm. Higher concentrations of iron show increased initial degradation, but the reaction remains stagnant in this series.

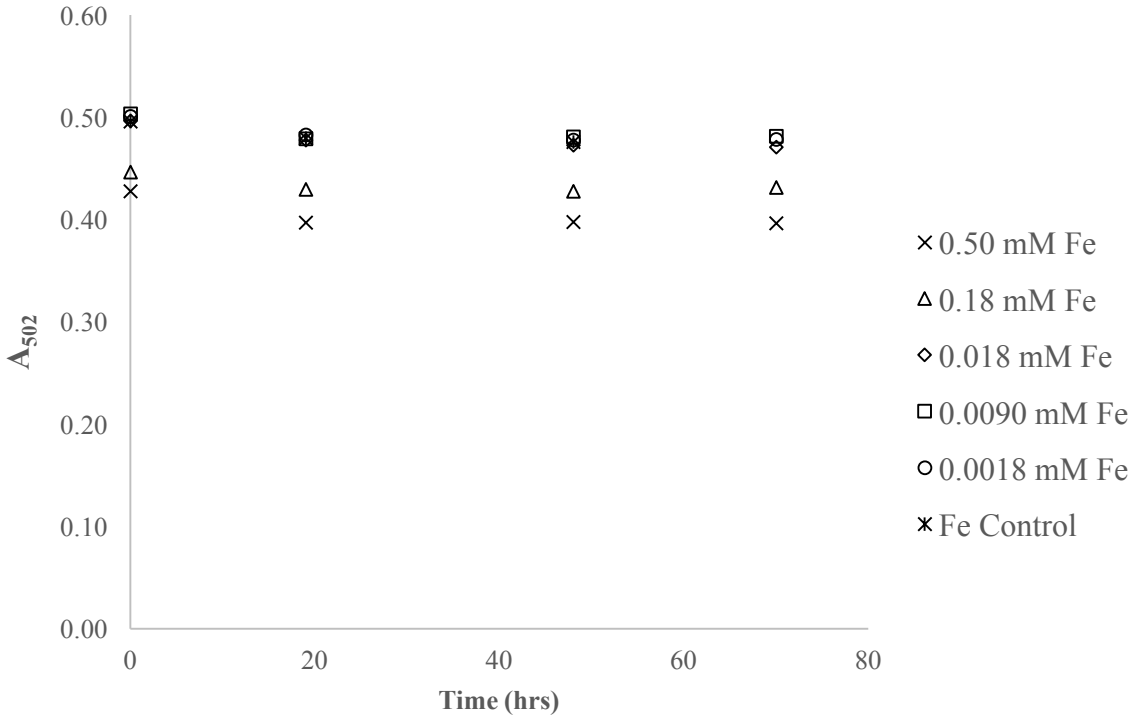

Figure 20. AR decolorization for buffered pH 5 iron series in 72 hours. This graph is a continuation from Figure 19. The absorbance remains relatively constant for each iron solution.

Given the possibility that the reaction ceases because a cloudy iron precipitate forms, making ferrous iron unavailable for catalysis, an inhibited reaction mixture was subsequently spiked with additional ferrous iron. Figure 21 shows the 0.50 mM iron pH 5 buffered solution which was spiked with an additional aliquot of 0.50 mM ferrous sulfate at 252,000 seconds. Absorbance decrease was apparent within 30 seconds after the addition, then again remained relatively constant over time.

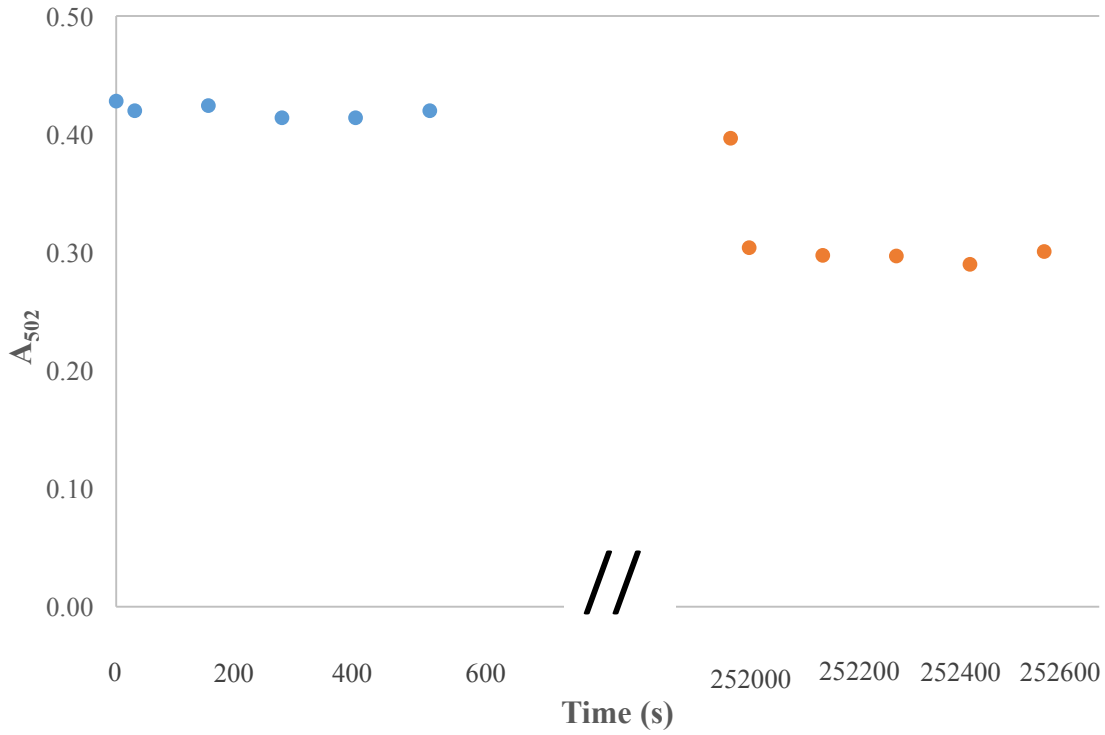

Figure 21. Kinetics of ferrous sulfate spike in pH 5 buffered solution. The depiction is incorporated from Fig. 19 at 70 hours (252,000 seconds). At approximately 252,000 seconds, a second aliquot of 0.50 mM iron was added to the reaction initially containing 0.50 mM iron.

The pseudo-first order rate constant for the pH 3 solution containing 0.50 mM iron was determined by taking the slope of the natural log of absorbance at 502 nm vs. time plot as shown in Figure 22. This method was used for all soluble iron series at different iron concentrations to compare pseudo-first order rate constants with iron concentration determined from ICP in Figure 23. Tables 1 and 2 display the pseudo-first order rate constant for each iron concentration in both pH 3 and 5 in DI water and in phosphate buffer.

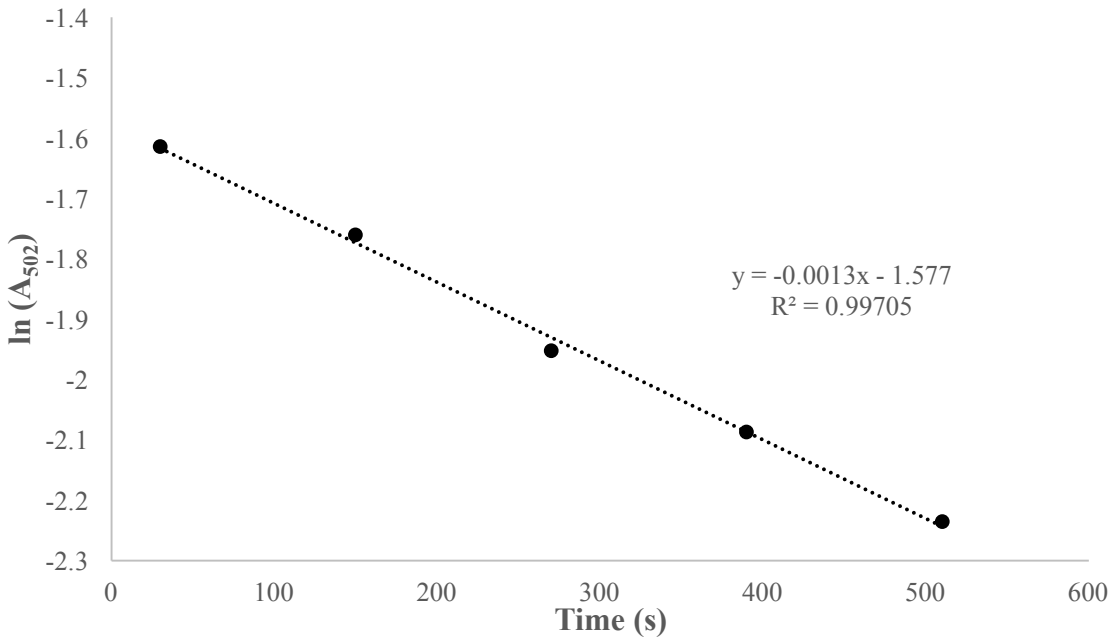

Figure 22. Pseudo-first order kinetic plot for pH 3, 0.50 mM Fe solution**.** The graph displays $\ln(A_{502})$ vs. time with a linear fit to determine the rate constant for the reaction in pH 3 solution containing 0.50 mM ferrous sulfate, 0.02 mM AR, and 9.98 mM hydrogen peroxide.

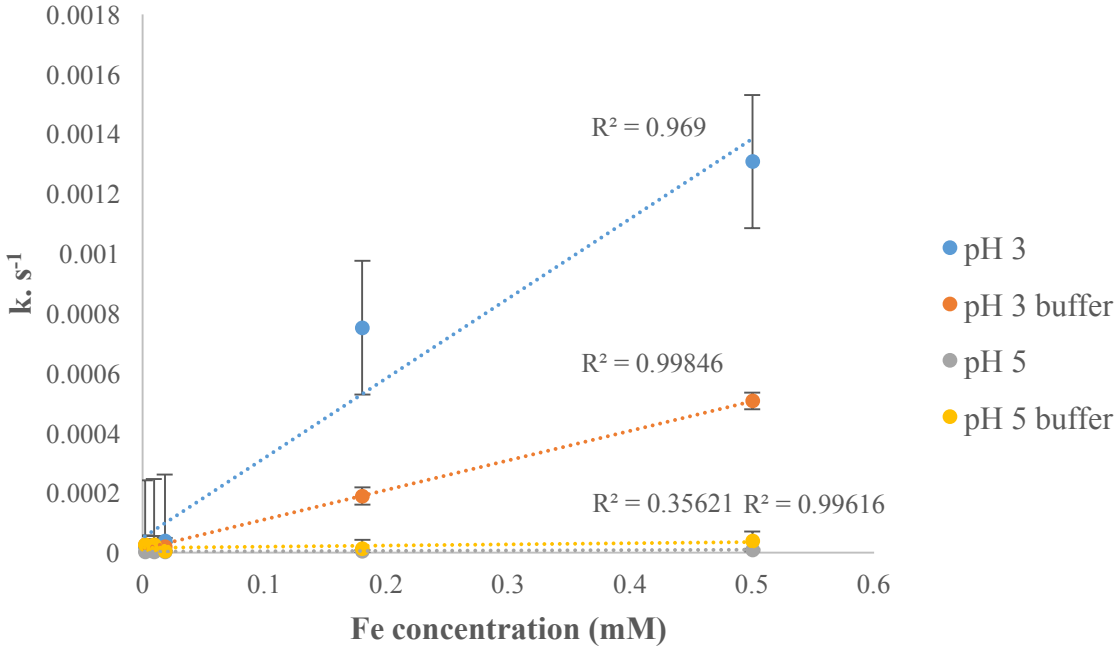

Figure 23. Pseudo-first order rate constant, k, vs. iron concentration for soluble iron series. The rate constant was determined for each iron concentration for pH 3, pH 3 buffer, pH 5, and pH 5 buffer.

pH 3			pH 5		
Iron (mM)	k	R^2	Iron (mM)	k	R^2
0.50	0.0013	0.99	0.50	8.9E-06	0.97
0.18	0.00075	0.99	0.18	5.1E-06	0.96
0.018	3.8E-05	0.99	0.018	2.9E-06	0.97
0.009	2.3E-05	0.99	0.009	2.8E-06	0.96
0.0018	2.0E-05	0.99	0.0018	2.4E-06	0.97

Table 1. Pseudo-first order rate constant, k, vs. ferrous sulfate concentration for unbuffered solutions. First order rate constant and correlation coefficient for each iron concentration in pH 3 and pH 5 solutions.

pH 3 buffer			pH 5 buffer		
Iron (mM)	k	R^2	Iron (mM)	k	R^2
0.50	5.1E-04	0.28	0.50	3.9E-05	0.36
0.18	1.9E-04	0.33	0.18	1.3E-05	0.05
0.018	2.0E-05	0.06	0.018	3.6E-06	0.005
0.009	1.7E-05	0.18	0.009	2.5E-05	0.38
0.0018	2.7E-05	0.29	0.0018	2.6E-05	0.63

Table 2. Pseudo-first order rate constant, k, vs. ferrous sulfate concentration for buffered solutions. First order rate constant and correlation coefficient for each iron concentration in pH 3 and pH 5 phosphate buffered solutions.

Immobilized Fenton Catalyst: Febpy PDMS

An iron crosslinked polymer network, Febpy PDMS, was used to degrade AR at near neutral pH. An absorption spectrum of the polymer dissolved in THF was measured with a peak absorbance at 538 nm as depicted in Figure 24.

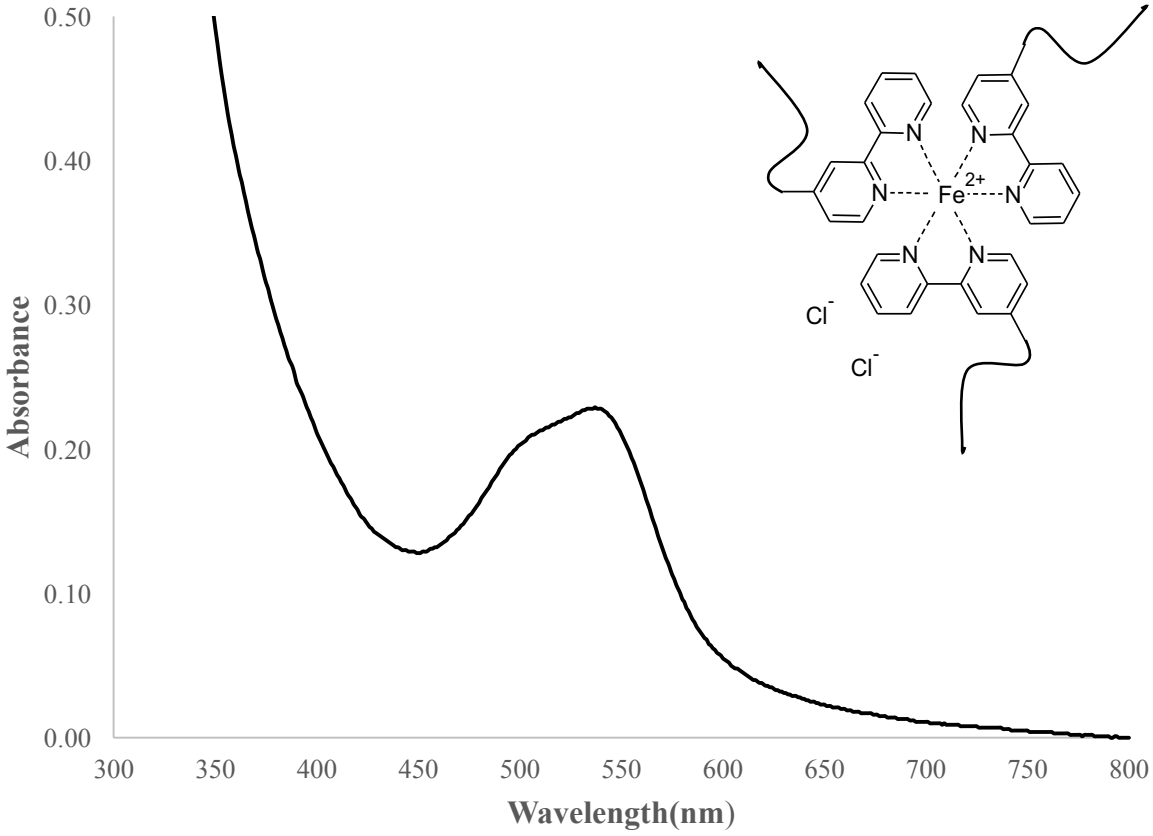

Figure 24. Febpy PDMS absorbance in THF. The absorption spectrum of the polymer indicates that the peak absorbance is at a similar wavelength of that of the peak absorbance of AR. Thanks to Dr. Al Schwab, Appalachian State, for the image of the polymer.

To determine the effectiveness of the Febpy PDMS immobilized catalyst in the degradation of AR, different amounts of catalyst were coated on round-bottom flasks in which the reaction took place. After 168 hours, the reaction flask coated with 200 uL Febpy PDMS experienced 67% dye removal, while the solutions coated from 100 uL or 500 uL of Febpy PDMS stock solution experienced 25% and 38% dye removal respectively as shown in Figure 25.

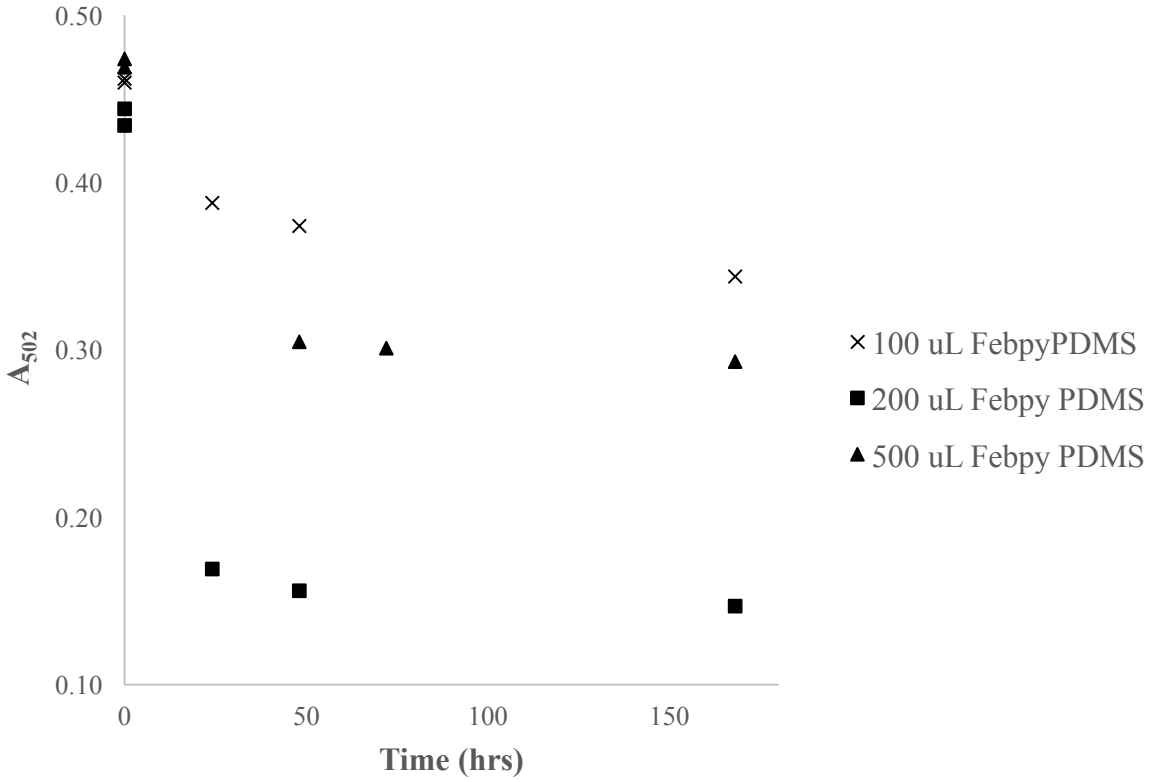

Figure 25. AR decolorization with immobilized Febpy PDMS catalyst. Three trials of the Fenton reaction in neutral buffered conditions with various volumes of Febpy PDMS stock solution used to coat the RBF. Each trial began upon the addition of hydrogen peroxide to a concentration of 9.98 mM in 25 mL of solution, and was stirred throughout the entire duration of 168 hours. Peak AR absorbance degradation was monitored at 502 nm. Approximately 0.02 mM of AR was used with 80 mM of pH 7 phosphate buffer with Febpy PDMS filmes deposited from 100 μL, 200 μL, or 500 μL of precursor solution.

After the Fenton reaction had occurred in each of the round bottom flasks, the filtrate was preserved and acid digested to quantify the concentration of iron that may have leached into solution. Samples were taken from the reactions that proceeded for one week. They were then acid digested along with a blank digest with nitric acid for 15 minutes and were transferred to acid washed round bottom flasks. Approximately 15 mL of nitric acid was added to each sample before being measured using ICP. An iron calibration curve was produced to determine the average triplicate iron concentrations, as depicted in Table 3, for each filtrate shown in Figure 26.

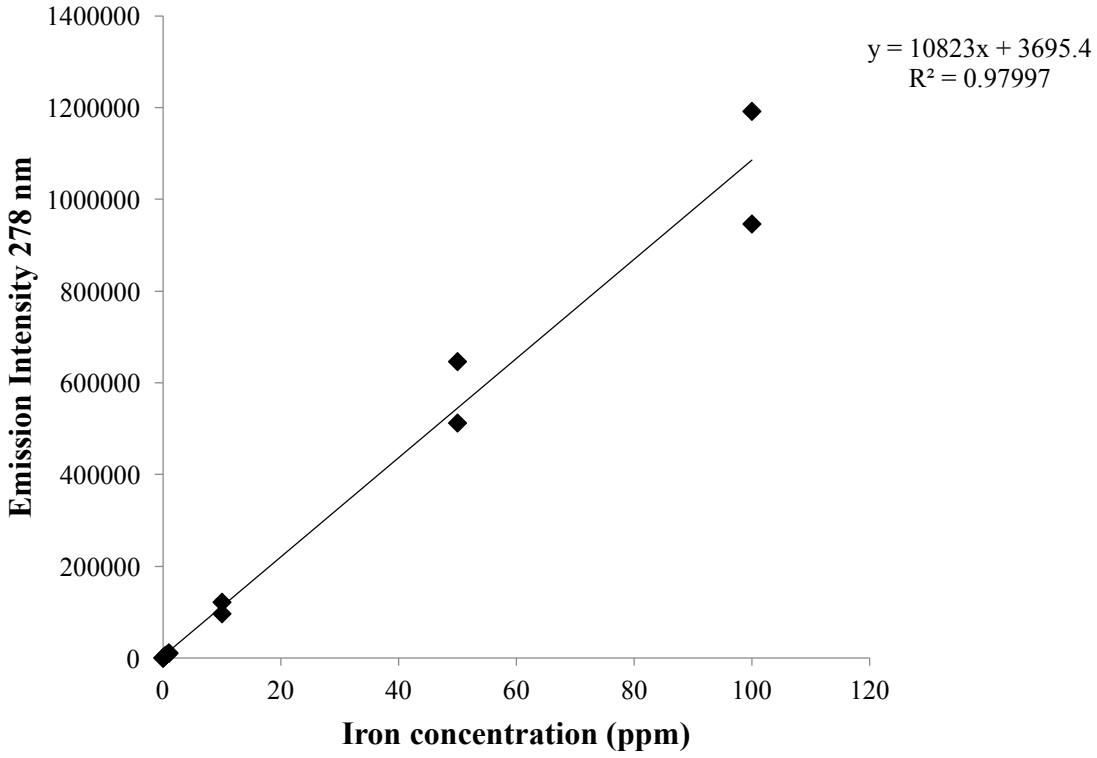

Figure 26. Iron calibration curve. The calibration curve was produced by measuring the emission at 278 nm for 0 ppm, 0.05 ppm, 0.5 ppm, 1ppm, 5ppm, and 50 ppm iron standards using ICP-OES. The calibration curve was then used to determine the iron concentration of the Febpy PDMS filtrates after undergoing the Fenton reaction. The standard error in the slope was 360.71.

Iron Sample	Average Iron Emission	Average Iron Concentration (ppm)	St Dev (+/-)
100 uL	557.13	0.05	0.88
200 uL	5837.42	0.54	0.88
500 uL	876.93	0.08	0.88
20 ppm LFB	228105.00	21.08	0.79
5 ppm IDL	60255.75	5.57	0.85

Table 3. Average triplicate iron concentrations of filtrate after Febpy PDMS treatment.

A second Febpy PDMS coating was applied to a RBF to further examine AR dye degradation at near neutral pH. After the reaction progressed for 168 hours, the solution was stored for ICP analysis. A replicate of the reaction was then initiated with the same polymer coating to test the feasibility of dye degradation for multiple uses, as depicted in Figures 27 and 28. In addition, an iron control, lacking any intentional source of iron, was used to determine if AR dye could be removed without polymer coating.

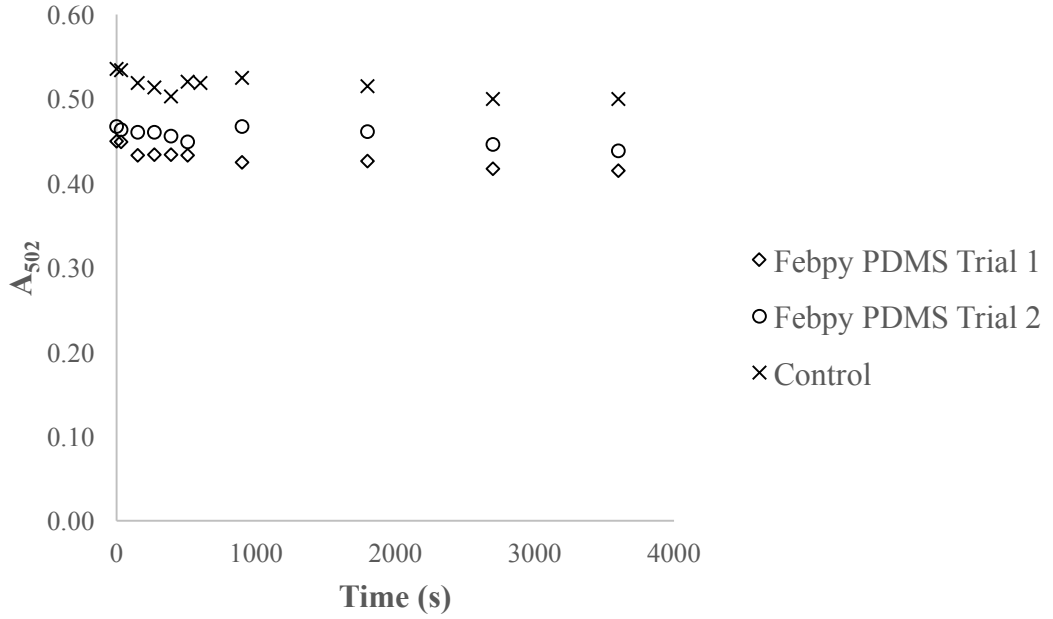

Figure 27. AR peak absorbance following treatment for one hour with immobilized Febpy PDMS. The 25 mL solutions contained 0.02 mM AR and all were initiated with 9.98 mM hydrogen peroxide at 30 seconds.

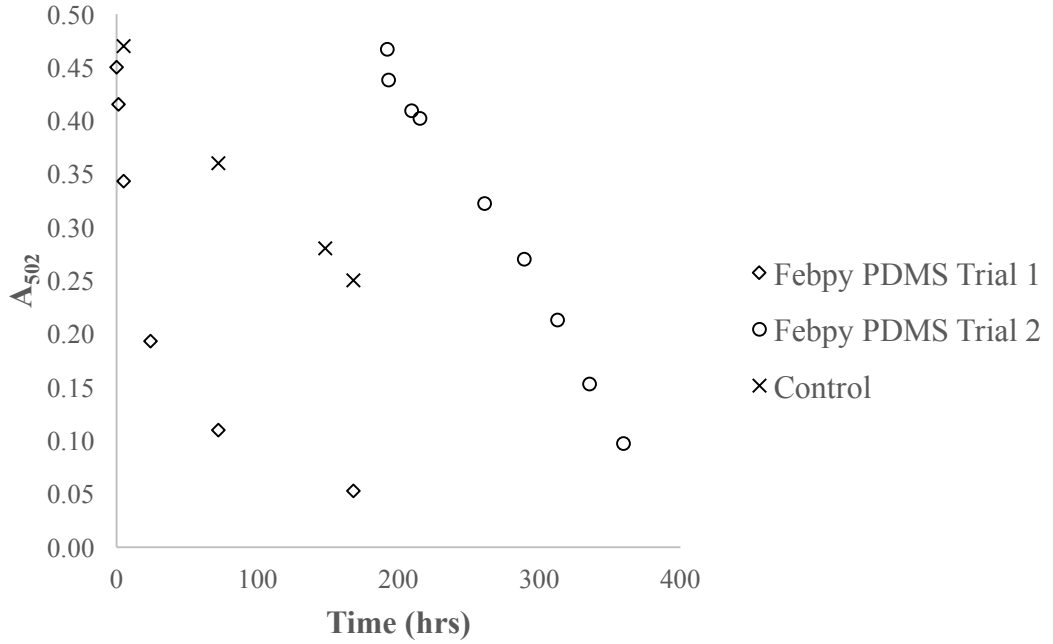

Figure 28. AR peak absorbance following treatment for one week with Febpy PDMS. A continuation of the trials in Figure 27. The Fenton reaction containing immobilized polymer demonstrated the highest AR removal for the first trial. AR was able to be removed for trial 2 containing the same polymer.

After examining the absorbance degradation from all solutions treated with Febpy PDMS polymer, it was determined that second order kinetics were favored over first order. Figure 29 shows the determination of the pseudo-second order rate constants for solutions treated with films of 100 µL, 200 µL, and 500 µL polymer based on the slope of a plot of $1/A_{502}$ vs. time. Pseudo-second order rate constants were determined for the replicate Febpy PDMS experiment in the same manner, as depicted in Table 4.

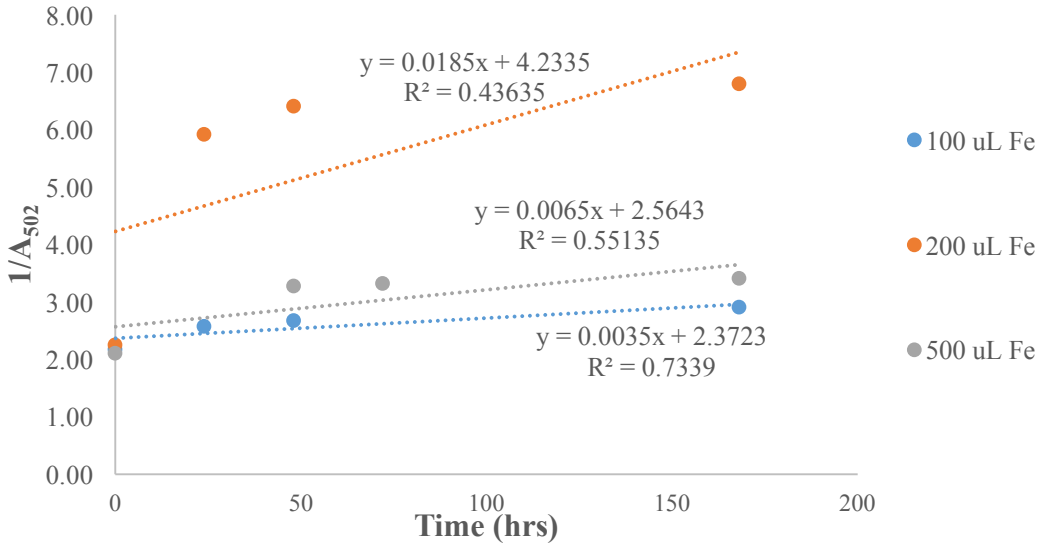

Figure 29. Pseudo-second order rate constants for Febpy PDMS treated solutions**.** The second order rate constant for each trial was determined by plotting the $l/(A_{502})$ vs. time and calculating the slope. The inverse absorbance values were variable as the reaction proceeded, as indicated by the low correlation coefficient values.

The second order rate constant was plotted against the amount of Febpy PDMS catalyst in Figure 30. Table 4 provides evidence for AR decolorization for the Febpy PDMS filtrate replicate. Overlaying the rate constants and iron concentration from all five trials of Febpy PDMS immobilized catalyst, it is evident that there is no correlation between the pseudo-second order rate constant and the amount of free iron in solution, as shown in Figure 31.

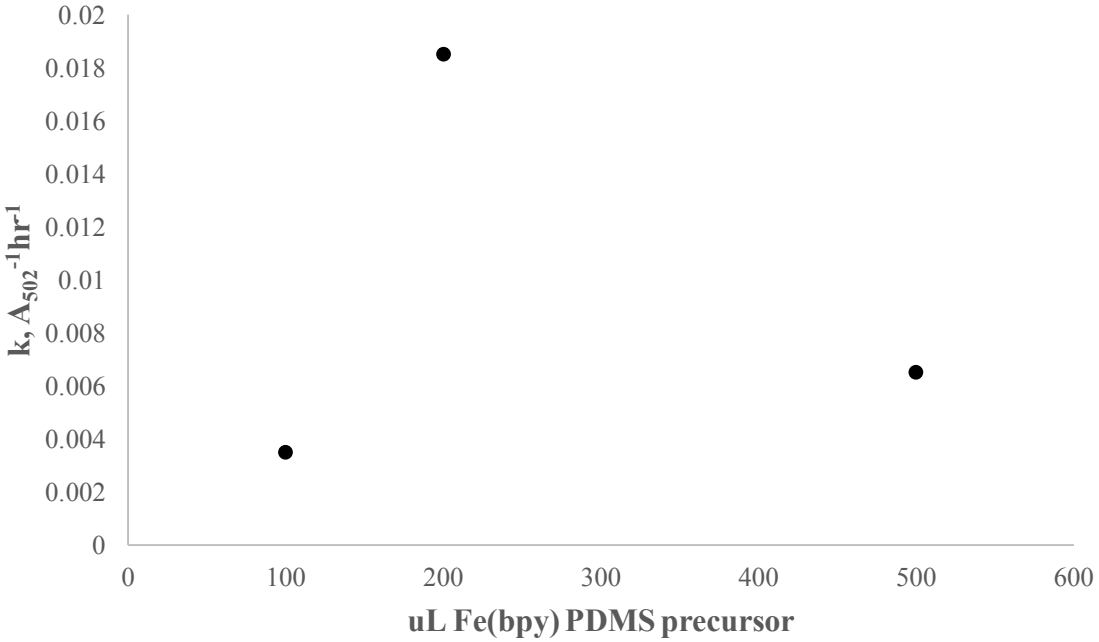

Figure 30. Pseudo-second order rate constants for 100 μL, 200 μL, and 500 μL Febpy PDMS solutions. The second order rate constant for each trial was determined by plotting the $l/(A_{502})$ vs. time graph and calculating the slope. These values are plotted against the amount of Febpy PDMS precursor used to coat the flask. The inverse absorbance values were variable as the reaction proceeded, as indicated by the low correlation coefficient values.

Sample	2nd order k, R^2	ICP iron concentration (ppm)	Standard Deviation
Febpy PDMS 1st Run	0.0977, 0.998	0.136	0.0013
Febpy PDMS 2nd Run	0.0377, 0.790	0.184	0.0011

Table 4. Pseudo-second order rate constant and average triplicate iron concentrations of second Febpy PDMS coated samples. The data indicates that the reaction rate is not dependent on iron concentration in solution.

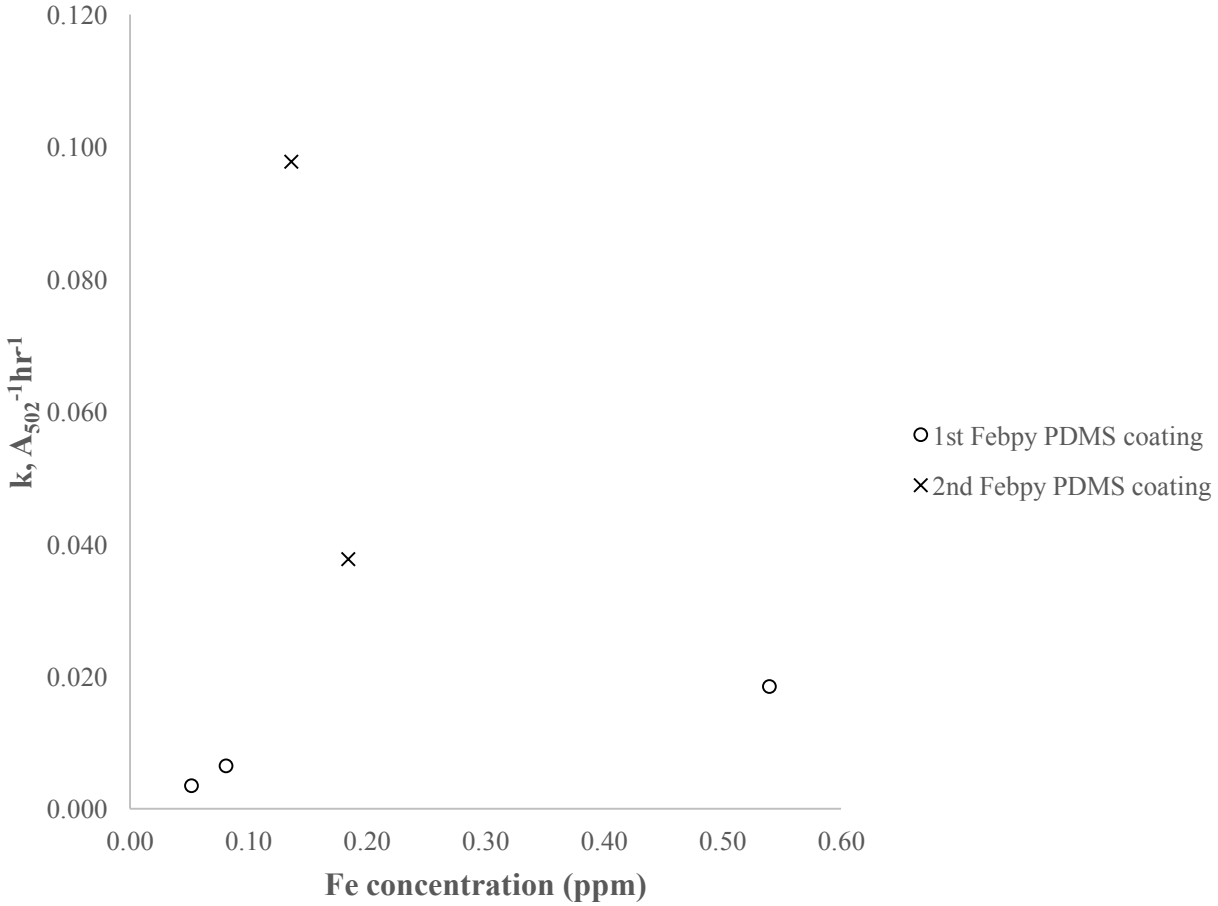

Figure 31. Pseudo-second order rate constant vs. iron concentration for all Febpy PDMS treated samples. The data shows a clear distinction between the rate of AR removal between the first the second coating of polymer. It is possible that the degradation of AR is not dependent on leaching of iron. The poor correlation between the pseudo-second order rate constant and the amount of iron in solution suggests that the degradation may vary depending on immobilized catalyst surface contact with hydrogen peroxide.

IR analysis of AR degradation

To further observe the degradation of AR, IR spectroscopy was used to analyze differences in chemical constituents of the compound before and after the Fenton reaction took place. Figure 32 shows an IR spectrum of solid AR. Peak assignments are made in Table 5.

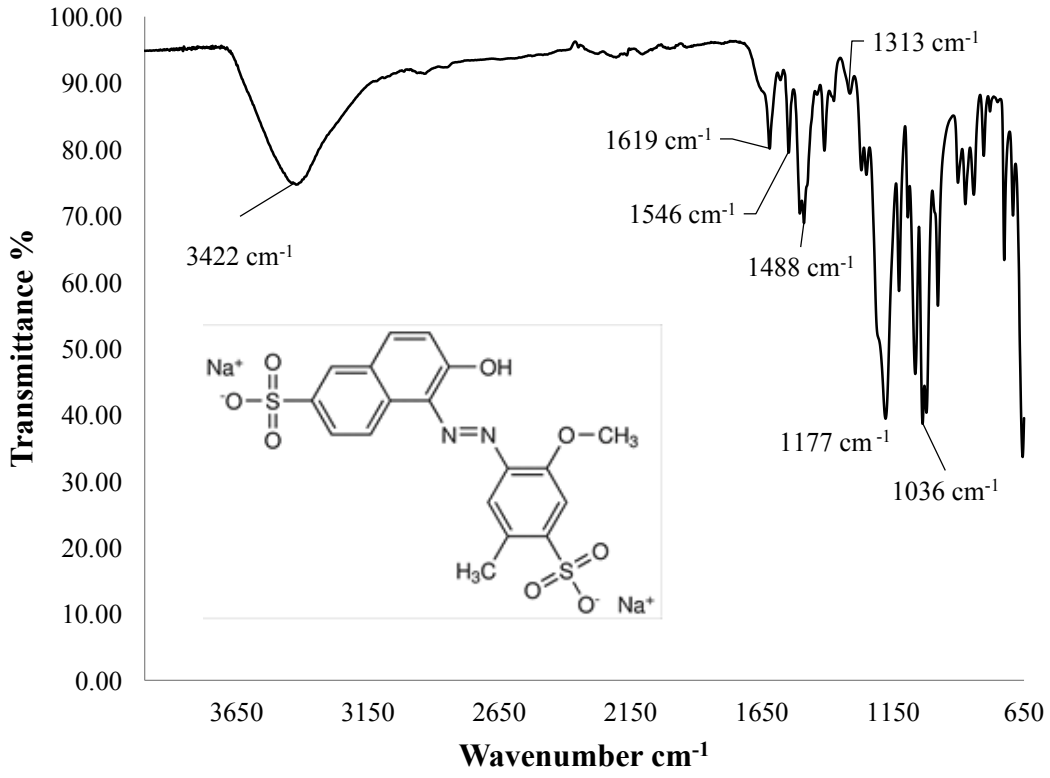

Figure 32. IR spectrum of solid AR. Peaks 3422 cm^{-1}, 1619 cm^{-1}, 1546 cm^{-1}, 1488 cm^{-1}, 1313 cm^{-1}, 1177 cm^{-1}, and 1036 cm^{-1} correspond to the different bond types present in the structure of AR. The compound on the bottom left of the IR spectrum is AR.

Wavenumber (cm^{-1})	Shape	Bond Type
1036.41, 1177.46	strong/sharp	Na salt of S=O
1313.21	weak/sharp	Asymmetric S=O
1488.32	medium/sharp	N=N
1546.36	medium/sharp	C=C
1619.12	medium/sharp	C=C
3422.85	strong/broad	O-H

Table 5. IR peak assignments for AR. The peak at 3422.85 cm^{-1} likely represents the O-H stretch of the phenol ring. Peaks at 1619.12 cm^{-1}, 1546.36 cm^{-1}, and 1488.32 cm^{-1} may be indicative of C=C and/or C=N bonds, and C=C and N=N bonds respectively. The S=O bonds in the molecule are likely being detected at 1313.21 cm^{-1}, 1177.46 cm^{-1} and 1036.41 cm^{-1}.

To monitor AR degradation during the Fenton reaction, aliquots of solution were measured using IR spectroscopy to monitor changes in chemical structure over time. The spectra of this aqueous reaction contained large peaks at 3310 cm^{-1} and 1640 cm^{-1}, which were indicative of the water solvent as shown in Figure 33.

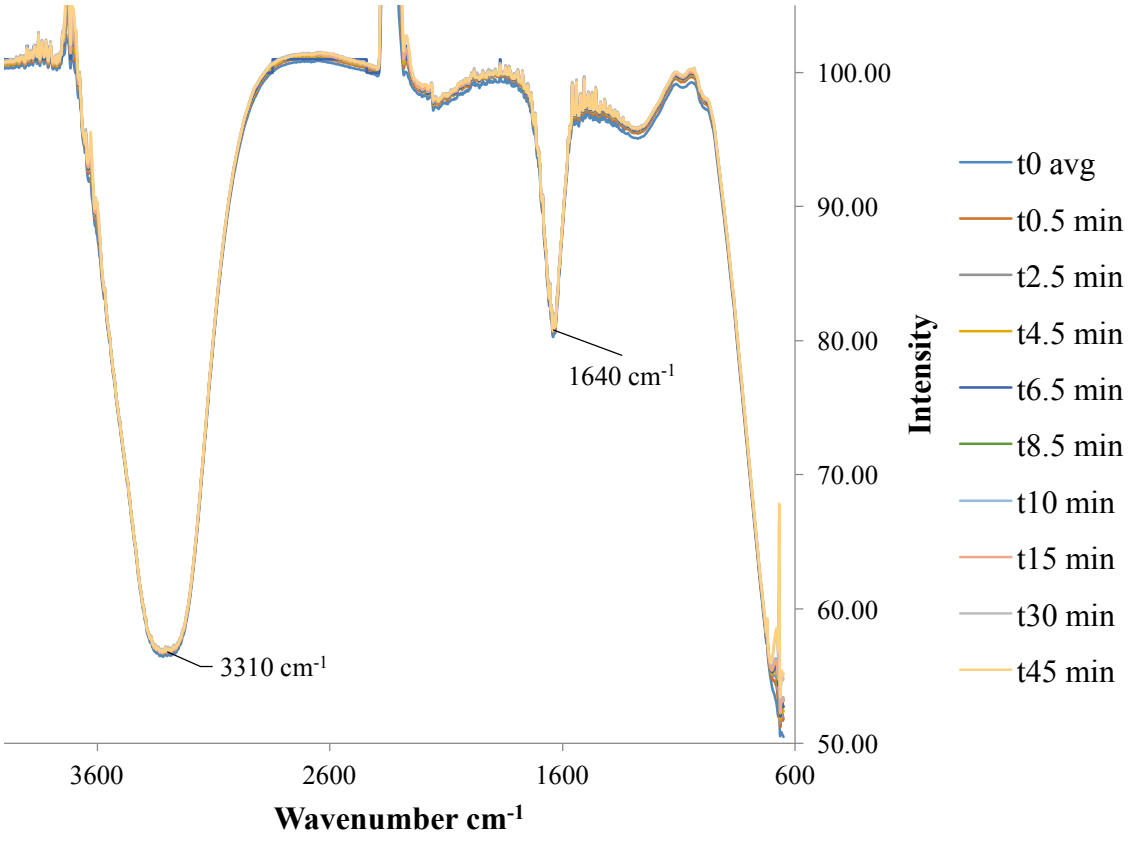

Figure 33. IR spectrum of aqueous AR solution during the Fenton reaction. The solution contained 0.5 mM Fe, 0.2 mM AR, and 9.98 mM of hydrogen peroxide.

The difference spectra were then calculated to determine which peaks were growing in as the reaction progressed as observed below in Figure 34-36. Positive peaks appearing on the difference spectrum indicate that the chemical bond is disappearing over the course of the reaction.

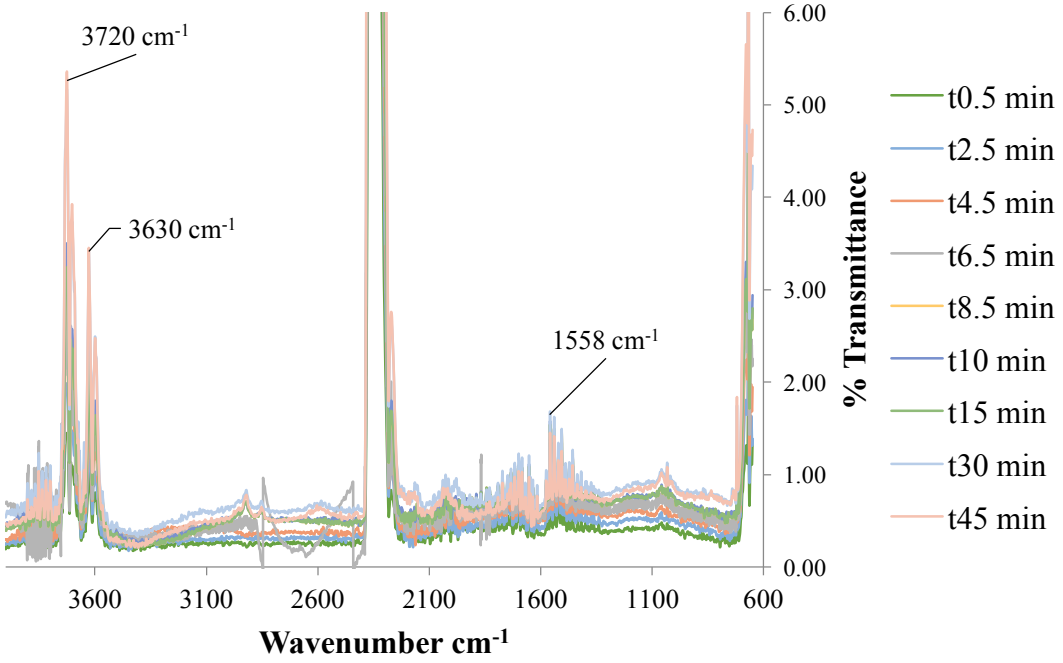

Figure 34. Difference spectra of AR solution during the Fenton reaction**.** It is evident that peaks at 3720 cm^{-1}, 3630 cm^{-1}, and 1558 cm^{-1}, experienced the greatest change during 45 minutes of the reaction.

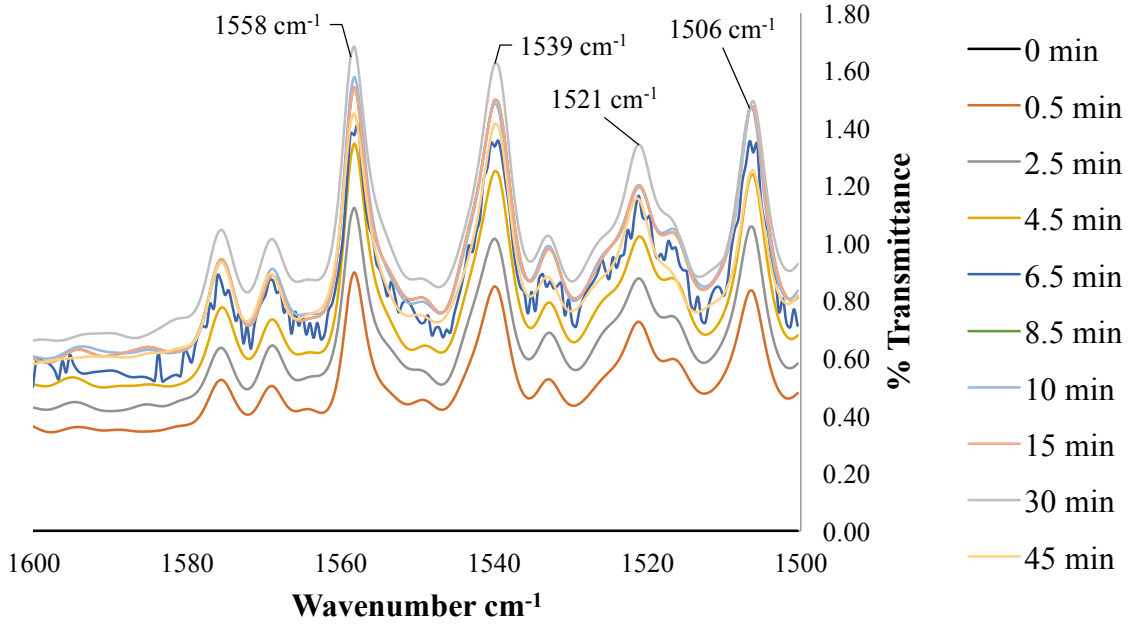

Figure 35. Difference spectrum of AR solution between 1500 cm^{-1} and 1600 cm^{-1}**.** This is an enlarged region of Figure 34. Peaks that experienced the greatest change over time were at 1558 cm^{-1}, 1539 cm^{-1}, and 1521 cm^{-1}, and 1506 cm^{-1} which may be indicative of C=C degradation of the aromatic rings in AR.

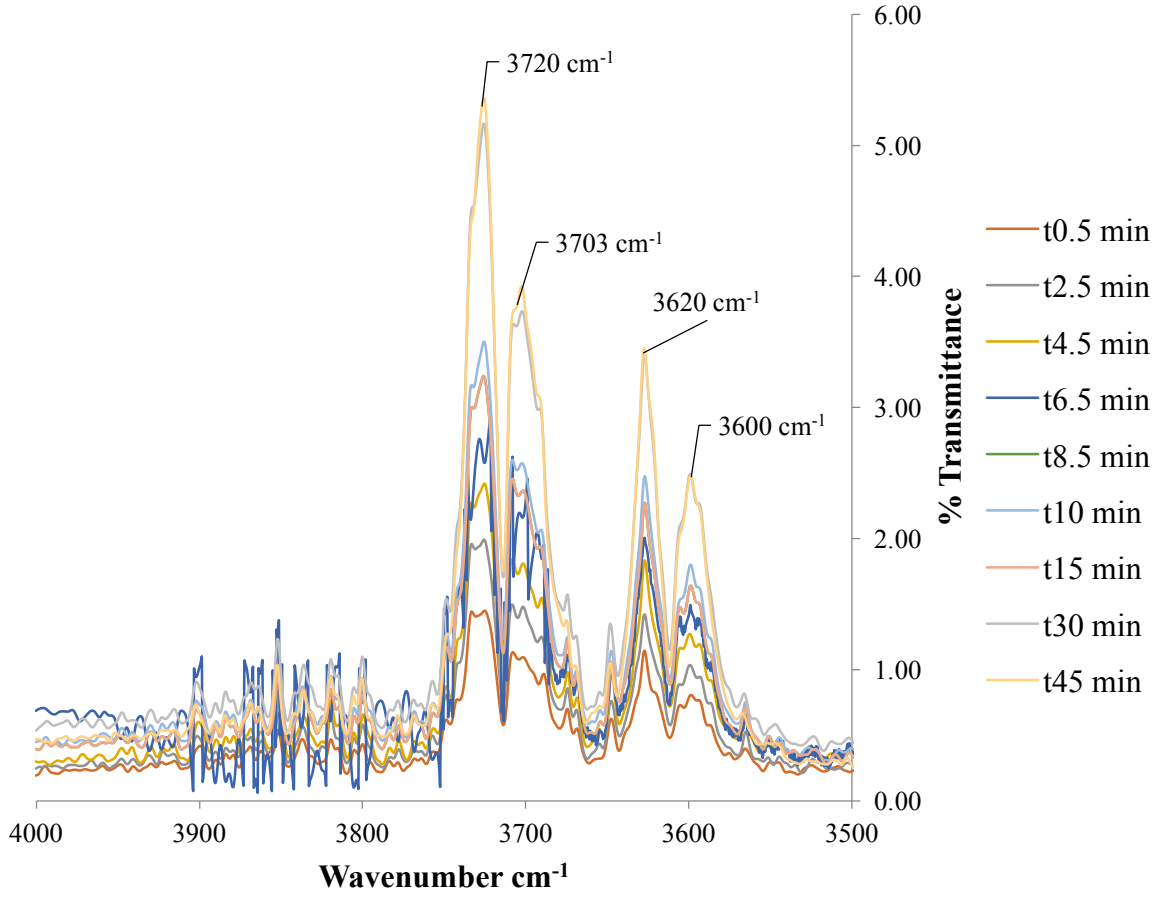

Figure 36. Difference spectrum of AR solution between 3500 cm^{-1} and 4000 cm^{-1}**.** This is an enlarged region of Figure 34. Peaks that experienced the greatest change over time were at 3726 cm^{-1}, 3703 cm^{-1}, and 3620 cm^{-1}.

The change in transmittance for peaks were then plotted against reaction time to determine which peaks experienced the largest change in transmittance. Figure 37 shows the increase in percent transmittance with time, and Table 6 indicates the peak assignments for each wavenumber.

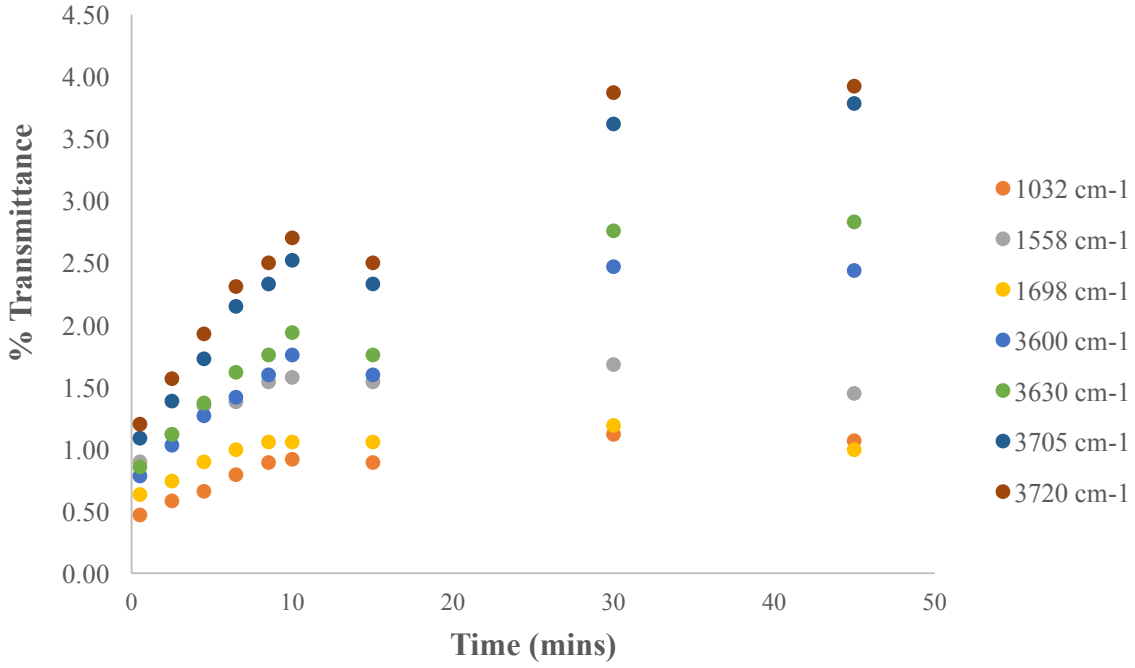

Figure 37. Change in transmittance over time for select peaks. This is an adaption from Figure 39. Examining the difference peaks, it is evident that 3720 cm^{-1} and 3705 cm^{-1} experienced the most change in 45 minutes of the Fenton reaction.

Wavenumber (cm^{-1})	**Shape**	**Bond Type**
1032	strong/sharp	Na salt S=O
1558	strong/sharp	C=C
1698	weak/sharp	C=C or C=N
3600, 3630	medium/sharp	Phenol free O-H
3705, 3720	medium/sharp	Sulfonic acid free O-H

Table 6. IR difference peak fitting for largest changes in transmittance. The peaks of most interest are 3720 cm^{-1}, 3705 cm^{-1}, 3630 cm^{-1}, 1698 cm^{-1}, 1558 cm^{-1}, 1032 cm^{-1}.

IV. Discussion

Preliminary Fenton Testing

After examining the extent of AR degradation at its peak wavelength of 502 nm using UV-vis spectroscopy, the data suggests that the reaction proceeds readily at pH 3 in the absence of buffer. This portion of work was undertaken to reassess the effect of pH and phosphate buffer on the reaction, since anomalous results had been recently reported in lab [24]. This new work clearly demonstrates that the Fenton reaction is not efficient at decolorization of AR at neutral pH, and also is less effective in the presence of phosphate buffer at lower pH. This poor performance is likely due to the oxidation of ferrous iron to ferric iron, and the subsequent precipitation of ferric iron from solution. The Fenton reaction cannot produce hydroxyl radicals and other reactive oxygen species rapidly without the catalyst remaining in contact with hydrogen peroxide in the aqueous phase. The Pourbaix diagram in Figure 3 further explains how unlikely it is for ferrous iron to be present at more neutral conditions. In the presence of high ferrous sulfate concentrations (0.98 mM), exponential scatter curves were apparent after the initiation of the reaction. The precipitation of ferric iron likely caused light to scatter off of the particles, causing a large scatter curve to develop. By subtracting the absorbance due to scattering at the peak wavelength of AR, the degradation of this dye could still be followed in these solutions.

The Fenton reaction was most successful in pH 3 in the absence of phosphate buffer. In the presence of phosphate buffer, pH 3, 5 and 7 solutions experienced absorbance decrease at the peak wavelength of AR in the first measurement interval of 30 seconds. After this, the absorbance remained constant over time. It is likely that iron (III) phosphate particles were precipitating out of solution. Iron (III) phosphate would be another way to remove iron from

solution, making it unavailable to catalyze the reaction. This precipitate was further isolated by filtration, washed with cold water, and dried at 120 °C. Comparing the IR spectra of the compound recovered in the reaction to the known spectrum of iron (III) phosphate provides supporting evidence for the assignments as iron (III) phosphate. The precipitation of this material from the reaction would similarly remove soluble ferrous iron from solution, inhibiting the reaction over time. In pH 5 phosphate buffer containing 0.50 mM ferrous sulfate, the solution experienced little degradation. After the reaction took place for 70 hours, the solution was spiked with an additional 0.50 mM of ferrous sulfate and AR degradation was noticed. Ten minutes following the iron spike, the absorbance was noticeably constant, which further supports the notion that phosphate buffered solutions were limited by the availability of catalytic iron.

Kinetics of the Homogeneous Fenton Reaction

Ferrous iron catalyst concentration has a direct impact on the rate of the Fenton reaction. High concentrations of iron (0.50 mM) in solution led to complete decolorization of AR in pH 3 solution. In the presence of phosphate buffer at both pH 3 and 5, the iron concentration played a role in the initial degradation of AR. Due to precipitation of iron(III) phosphate material, ferrous iron was limited in both solutions, which likely prevented the production of reactive oxygen species to further degrade AR.

The pseudo-first order rate constants from all solutions demonstrated a positive correlation with the ferrous iron concentration in solution. As observed in Figure 23, the pH 3 solution in the absence of buffer had the largest rate constant while the pH 5 solution in buffer had the lowest rate constant. This is likely because ferrous iron is the more active form of the Fenton catalyst [26], and it is not being regenerated at a fast rate in more neutral pH in

the presence of phosphate. Both pH 3 and 5 solutions in the absence of buffer experienced gradual absorbance degradation with time, while the rate of the reaction for buffered solutions were mostly stunted after 30 seconds. This strongly suggests that phosphate buffer should not be used in the degradation of AR in homogeneous solution, due to the dependence on ferrous iron.

Immobilized Febpy PDMS

The heterogeneous Fenton reaction is more useful in waste water purification as it requires less steps during the treatment process. In the homogeneous Fenton reaction, a reduced soluble first row transition metal is required to catalyze the reaction, and this material must be removed before effluent is released [22]. In addition, the pH of the effluent would have to be raised to neutral, which can be more expensive. Applying an immobilized catalyst to the reaction chamber will prevent the need for filtration and pH adjustment after pollutant degradation, making this application more appealing and affordable.

An iron crosslinked polymer network, Febpy PDMS, was used to coat the walls of RBF to provide a suitable catalytic surface to degrade organic pollutants at neutral pH. The parent $[Fe(bpy)_3]^{2+}$ soluble complex, and derivatives, have been used as homogeneous catalysts in mineralizing model organic pollutants such as azo dye orange (II) and 2,4-dichlorophenol [27]. These catalysts also have been tested in the heterogeneous reaction after immobilization on high surface area clay zeolites [28], and are able to degrade organic materials under visible irradiation [29]. In this work, solid Febpy PDMS polymer was explored as an alternative heterogeneous Fenton catalyst for the removal of AR. After the reaction proceeded in reaction flasks containing different amounts of coated Febpy PDMS, it was evident that there was no correlation with the amount of coated polymer and AR

removal (Figure 30). The AR solution treated with a coating prepped from 200 μL experienced the greatest degradation of the pollutant. After the filtrates were collected, filtered, and acid digested, the iron concentrations were determined using ICP. These results indicate that the filtrate from the 200 μL coated RBF contained the largest amount of ferrous iron in solution. Elevated concentrations of ferrous iron in solution strongly suggest this ion was leaching out of the heterogeneous coating and into solution. The leaching of catalyst would provide a source of free iron to drive the homogeneous Fenton reaction. However, AR degradation within the second coating of Febpy PDMS showed a higher pseudo-second order rate constant of 0.0977, while the filtrate contained 0.136 ppm of ferrous iron as shown in Table 4. In comparison to the decolorization of AR in the 200 μL coating of Febpy PDMS, the pseudo-second order rate constant was 0.0185 as depicted in Figure 29, with 0.54 ppm of ferrous iron in the filtrate as shown in Table 3. Since the pseudo-second order rate constant was higher for the solution contained within the second coating of Febpy PDMS, and there was less free iron present in the filtrate, it is likely that AR is not solely being degraded from leached iron in solution. This suggests some catalytic activity for the immobilized Febpy PDMS material. To tentatively explain the variable performance for this material, it is worth noting that the Febpy PDMS polymer was not uniformly coated onto the RBF, therefore it is likely that AR is being removed at different rates depending on the amount of iron coming into contact with hydrogen peroxide in the heterogeneous Fenton reaction. The second coating of polymer in near neutral pH demonstrated successful degradation of AR in one week with 88% removal. Reuse of the catalyst was effective in degrading the pollutant for at least one additional trial, however, the rate of decolorization was modestly slower.

IR Analysis of AR Degradation

In addition to UV-vis spectroscopy, other methods were desired to monitor the degradation of AR. UV-vis spectroscopy can only detect absorbance removal during the Fenton reaction. Since decolorization of the dye can occur early in the sequence of reactions leading to complete mineralization of carbon, further analysis of AR degradation was in order. Chemical oxygen demand (COD) was attempted initially, but it was noticed that the presence of hydrogen peroxide interfered with COD detection. This was verified in literature, with the oxidation of hydrogen peroxide by dichromate shown as a known source of COD interference [30] Therefore, IR spectroscopy was used as a second method for monitoring AR degradation in the chemical structure. The IR difference spectra, which were produced by subtracting the initial AR spectrum from spectra taken throughout the progression of the reaction, contained multiple peaks. In the difference spectra, positive peaks corresponding to a decreased abundance of a specific functionality, were observed mostly between 3600 cm^{-1} and 3750 cm^{-1}, and between 1450 cm^{-1} and 1600 cm^{-1}. Based on these wavenumber ranges and examining the structure of AR, it may be possible that the compound was being broken down at the O-H bond within the phenol ring, at the S=O bond, and at C=C bonds in the aromatic ring. It is possible that the peaks at 3720 cm^{-1} and 3630 cm^{-1} were indicative of free O-H bonds due to the degradation of the underlying chemical functionality which was not observed in the IR spectra of pure AR solid. The solid shows a broad O-H stretch of the intermolecular hydrogen bonded system, while the difference spectra may have allowed us to see the loss of the underlying free O-H bonds. Intramolecular hydrogen bonding of the phenol O-H to the lone pair of electrons on the N=N bond may also be occurring within the structure. The change in transmittance for multiple wavenumbers shown in Figure 37,

supports the notion that the molecule was being broken down at several locations. The finding is not unexpected given the highly oxidizing, and hence relatively non-specific, nature of the hydroxyl radical.

V. Future Work

The Fenton reaction is an appropriate solution for organic pollutant removal from waste water. Both the soluble and immobilized iron catalysts are successful in degrading the model AR dye, but the immobilized catalyst does not depend on the solubility of iron. This is advantageous for contaminant removal at neutral pH, as the catalytic surface is mostly maintained during the reaction. It is important to consider that though the homogeneous Fenton reaction cannot proceed at neutral pH, it reacts at a much faster rate in low pH.

To further evaluate the Fenton reaction as a mechanism for tertiary wastewater treatment, improvements would need to be made for solutions utilizing both catalysts. The catalytic material must be filtered out of solution before releasing effluent for the homogeneous Fenton reaction. Deposition of the immobilized catalyst should be modified to prevent iron from leaching into solution. In addition, the reaction rate is slow for the immobilized catalyst, which may be due to the limited surface contact with the iron in the polymer and hydrogen peroxide to produce reactive oxygen species. This limitation could be addressed by coating multiple RBFs with various thicknesses of material. The entirety of this experiment was performed using either DI water or phosphate buffer in solution, though waste water will contain a more complex media. Due to this difference, the Fenton reaction may not be as efficient at removing AR or other organic pollutants from waste water as it would in DI water.

Other instrumentation, such as total organic carbon (TOC) and liquid chromatography-mass spectrometry could be used to more fully monitor the degradation of organic pollutants in waste water to determine the extent of mineralization. Though UV-vis spectroscopy is useful in tracking absorbance removal with time during the reaction, it does not investigate the potential for uncolored byproducts to be produced. Further computational methods associated with IR spectra may also provide a more complete picture of which chemical constituents are being targeted during the Fenton reaction.

VI. Conclusions

The demand for clean and accessible water in both developed and developing countries is likely to become even more pronounced in future years. Fenton chemistry, among several other advanced oxidation processes, can be employed in WWTPs to efficiently degrade organic pollutants from water at an affordable cost. Though the Fenton reaction proceeds readily at low pH in homogeneous solution, the soluble catalyst cannot be used in the removal of AR at neutral pH. Further research needs to be conducted on removing contaminants at neutral pH to limit the number of steps in the water treatment process. Phosphate buffer should not be used in the Fenton reaction, as it interferes with the interaction between ferrous iron and hydrogen peroxide to generate reactive oxygen species. The AR compound appears to be degraded at multiple locations when undergoing the Fenton reaction, specifically at the O-H bond in the phenol ring, the sulfonate group, and at aromatic C=C bonds and connecting C-N bonds. Immobilized Febpy PDMS seems promising as a heterogeneous catalyst for tertiary treatment, and should be further explored in removing organic contaminants from waste water.

Acknowledgements

I would like to thank Dr. Al. Schwab for providing the bpyPDMS necessary to synthesize the heterogeneous catalyst. Also, I would like to thank Hayden Lane for assistance in simulation of FTIR spectra.

References

1. Mekonnen, M.; Hoekstra, A., Four billion people facing severe water scarcity. *Science advances* **2016**, *2* (2), 1-6.
2. *Drinking-water Fact Sheet;* World Health Organization: November 2016. http://www.who.int/mediacentre/factsheets/fs391/en/. Accessed April 2017.
3. Alcamo, J.; Florke, M.; Marker, M., Future long-term changes in global water resources driven by socio-economic and climatic changes. *Hydrological Sciences Journal* **2010,** *52* (2), 247-275.
4. Perlman, H., The Water Cycle: Freshwater Storage. https://water.usgs.gov/edu/watercyclefreshstorage.html. Accessed March 2017.
5. Bates, B.C., Kundzewicz, Z. W.; Wu, S.; Palutikof, K.P., Chapter 2: Observed and projected change in climate as they relate to water. In: *Climate change and water*. IPCC Secretariat, Geneva, **2008.** https://www.ipcc.ch/publications_and_data/_climate_change_and_water.htm.
6. Barnett, T. P.; Pierce, D. W.; Hidalgo, H. G.; Bonfils C., Human-induced changes in the hydrology of the Western United States. *Science* **2008,** *319*, 1080-1083.
7. Koutsoyiannis, D.; Zarkadoulas N.; Angelakis, A. N.; Tchobanoglous, G., Urban water management in ancient Greece: Legacies and lessons. *Water Resources Planning and Management* **2008**, *134* (1), 45-54.
8. Lankao, P. R., How do local governments in Mexico City manage global warming? *The International Journal of Justice and Sustainability* **2007,** *12* (5), 519-535.
9. Konikow, L.F., 2013, Groundwater depletion in the United States (1900−2008): U.S. Geological Survey Scientific Investigations Report **2013**-5079. http://pubs.usgs.gov/sir/2013/5079.
10. Kolpin, D. W.; Furlong, E. T.; Meyer, E.; Thurman, M.; Zuagg, S. D.; Barber, L. B.; Buxton, H. T., Pharmaceuticals, hormones, and other organic wastewater contaminants in U.S. streams, 1999-2000: A national reconnaissance. *Environmental Science & Technology* **2002,** *36* (6), 1202-1211.
11. Development of the Clean Water Act and the NPDES Program. In *NPDES Permit Writers' Manual*, U.S. Environmental Protection Agency, Ed. 2010;
12. Zhao, Y.; Hu, I.; Jin, W., Transformation of oxidation products and reduction of estrogenic activity of 17beta-estradiol by a heterogeneous photo-Fenton reaction. *Environmental Science & Technology* **2008,** *42* (14), 5277-5284.
13. Hao, O. J.; Kim, H.; Chiang, P., Decolorization of wastewater. *Critical Reviews in Environmental Science and Technology* **2010,** *30* (4), 449-505.

14. Grady C. P.; Daigger, G. T.; Love, N. G.; Filipe, C. D. M., *Biological Wastewater Treatment, Third Edition*. IWA: Boca Raton, Fl, 2011.
15. Fenton, H. J. H., Oxidation of tartaric acid in presence of iron. *Journal of the Chemical Society, Transactions* **1894,** *65*, 899-910.
16. Haber, F.; Willstatter, R., Unpaarigkeit und radikalketten im reaktionsmechanismus organischer und enzymatischer Vorgänge. *European Journal of Inorganic Chemistry* **1931**, *64* (11), 2844-2856.
17. Martinez-Huitle, C. A.; Brillas, E., Decontamination of wastewaters containing synthetic organic dyes by electrochemical methods: A general review. *Applied Catalysis B: Environmental* **2009,** *87* (3-4), 105-145.
18. Sabhi, S.; Kiwi, J., Degradation of 2,4-dichlorophenol by immobilized iron catalysts. *Water Research* **2001,** *35* (8), 1994-2002.
19. Ruppert, G.; Bauer, R., The photo-Fenton reaction - an effective photochemical wastewater treatment process. *Photochemistry and Photobiology A: Chemistry* **1993,** *73* (1), 75-78.
20. Delahay, P.; Pourbaix, M.; Rysselberghe, P., Potential-pH diagrams. *Journal of Chemical Education* **1950,** *27* (12), 683-688.
21. Barbusinksi, K., Fenton reaction - controversy concerning the chemistry. *Ecological Chemistry and Engineering S* **2009,** *16* (3), 348-358.
22. Neyens, E.; Baeyens, J., A review of classic Fenton's peroxidation as an advanced oxidation technique. *Journal of Hazardous Materials* **2003,** *98* (1-3), 33-50.
23. Yamamoto, N.; Koga, N.; Nagaoka, M., Ferryl-oxo species produced from Fenton's reagent via a two-step pathway: minimum free-energy path analysis. *The Journal of Physical Chemistry B* **2012,** *116* (48), 14178-14182.
24. Edge, C. M.S Thesis, Appalachian State University, Boone, NC, Dec 2015.
25. Salah A. Ait; Jozwiak, P.; Zaghib, K.; Garbarczyk, J.; Gendron, F.; Mauger, A.; Julien, C.M., FTIR features of lithium-iron phosphates as electrode materials for rechargeable lithium batteries. *Spectrochimica Acta Part A* **2006,** *65* (5), 1007-1013.
26. Pignatello, J. J.; Oliveros, E.; Mackay, A., Advanced oxidation processes for organic contaminant destruction based on the Fenton reaction and related chemistry. *Critical Reviews in Environmental Science and Technology* **2006**, *36* (1), 1-84.
27. Xi, C.; Wanhong, M.; Jing, L.; Zhaohui, W.; Chuncheng, C.; Hongwei, J.; Jincai, Z., Photocatalytic oxidation of organic pollutants catalyzed by an iron complex at biocompatible pH values: using O_2 as main oxidant in a Fenton-like reaction. *The Journal of Physical Chemistry C* **2011,** *115* (10), 4089-4095.
28. Bossmann, S. H.; Shahin, N.; Thanh, H. L.; Bonfill, A.; Worner, M.; Braun, A. M., $[Fe_2(bpy)_3]^{2+}$/ TiO_2-codoped zeolites: synthesis, characterization, and first application in photocatalysis. *ChemPhysChem* **2002,** *3* (5), 401-407.
29. Cheng, M.; Ma, W.; Chen, C.; Yao, J.; Zhao, J., Photocatalytic degradation of organic pollutants catalyzed by layered iron(II) bipyridine complex-clay hybrid under visible irradiation. *Applied Catalysis B: Environmental* **2006,** *65* (3-4), 217-226.
30. Talinli, I; Anderson, G. K., Interference of hydrogen peroxide on the standard COD test. *Water Research* **1992,** *26* (1), 107-110.